

University of Twente
**Faculty of Electrical Engineering,
Mathematics and Computer Science**

Graduation Thesis

**Epoxy-ceramic based NTC temperature
sensors for improved humidity stability
and low curing temperatures**

Submitted by

Joel Benavides Hatakeda (s2621673)

Course of

MSc. Electrical Engineering

August 2022

External Supervisor:

Dr. Peter Zalar

Internal Supervisor:

Dr. Ir. R.J. Wiegerink

Thesis Organization:

TNO

ABSTRACT

Temperature measurements are used in many industrial applications as a tool for controlling or monitoring a process. In batteries, temperature is an important parameter to make sure the charge and discharge is performed efficiently and, thus, enlarge the lifetime of the device.

Holst Centre developed a flexible printed NTC thermistor, based on a Manganese-Nickel ceramic dispersed on a polymer matrix, that has the accuracy as well as the electrical and mechanical performance needed for such task but presents 2 main disadvantages: only PI films are used as flexible substrate because of the curing temperature of the NTC composite (above 200 °C) and performance of the sensor is affected by humidity.

A solution based on an epoxy-ceramic composite was presented to tackle the issues mentioned above. The implications of changing the polymer in the formulation were studied by assessing the percolation limit of the new composite and understanding the influence of pressure as well as the electrode design. Humidity stability was tested based on the properties of the epoxy and the electrode material.

Results showed that the epoxy permitted lowering down the curing temperature of the NTC ink (down to 180 °C) which allowed to increase the range of materials to be used as flexible substrates (PEN, PET). Influence of humidity in the sensor's performance decreased with the new composite but is still present (changes in thermistor's resistance due to humidity, but not temperature, are above 1%).

Further optimization of the formulation or an external humidity barrier should be considered for future works.

ACKNOWLEDGEMENT

I would like to give special thanks to TNO's Holst Centre for letting me be part of this project and providing all the facilities for the tests needed, to my supervisors Dr. Peter Zalar and Dr. Akchheta Karki for guiding me throughout this assignment and to my university's supervisor Dr. Ir. R. J. Wiegerink for providing the feedback on my progress and making sure it was up to the standards of the University of Twente.

CONTENTS

- Abstract** **i**

- Acknowledgment** **ii**

- 1 Introduction** **1**
 - 1.1 Problem Background 3

- 2 NTC thermistor** **6**
 - 2.1 Structure 6
 - 2.2 Characteristics 7
 - 2.3 Conduction mechanism 9
 - 2.4 Holst Centre’s novel composite thermistor 10
 - 2.4.1 Material processing and preparation 10
 - 2.4.2 NTC ink mixture 12
 - 2.4.3 Issues 12
 - 2.5 Epoxy-ceramic based NTC thermistor 15
 - 2.6 Research questions for an epoxy-ceramic based NTC temperature sensor 15

- 3 Methods** **17**
 - 3.1 Functional granular composites 19
 - 3.1.1 Composite model 22
 - 3.2 Particle-to-particle contact 24
 - 3.2.1 Constriction resistance 24
 - 3.2.2 Tunneling resistance 25
 - 3.2.3 Deformation dependent resistance 25
 - 3.3 Electrode geometry effect on resistivity and connectivity of the NTC temperature sensor 27
 - 3.4 Humidity stability 29

4	Results	32
4.1	Percolation limit	32
4.2	Pressure influence	34
4.3	Electrode design influence	36
4.4	Humidity stability	37
5	Discussion	39
5.1	Percolation limit	39
5.2	Pressure influence	40
5.3	Electrode influence	40
5.4	Humidity stability	41
6	Conclusions	42
	References	43

1 INTRODUCTION

Measurement of temperature, for its monitoring or control, is an important task for domestic as well as industrial applications. It has an impact in different fields like health (human body temperature can determine its health condition), material processing (reach melting point in metals, reach enough temperature for thermoforming in plastics), food or beverage processing (linked to its quality and as an important factor for bulk production), electronic systems (monitoring of the device's condition), etc.

Temperature can be understood as the average kinetic energy of atoms or molecules in a system. Its measurement is normally done indirectly by assessing the change of a physical property of the material that changes with temperature. For example, in a mercury-in-glass thermometer, the working fluid, mercury, expands as temperature increases and a temperature value can be obtained depending on the volume expansion inside the glass tube.

Several different sensors were developed to properly measure temperature through different physical properties though the characteristics of each device differ in terms of accuracy, range, sensitivity, etc. The selection of a specific device will depend on the application's requirements.

These sensors can be divided in 4 general types: thermistors, thermocouples, integrated circuits and RTDs (resistance temperature devices). Below on table 1.1, it can be seen a comparison between these devices [1][2].

Table 1.1: Performance overview of different temperature sensor types.

Characteristics	Thermistors	Thermocouples	Integrated circuits	RTDs
Range (°C)	-50 to 250	-270 to 2000	-50 to 150	-200 to 650
Linearity	Exponential	Nonlinear	Linear	Linear
Response time (s)	Fast (0.1 to 10)	Fast (0.1 to 10)	Fastest (below 0.1)	Slowest (1 to 50)
Accuracy (\pm °C)	0.01 to 1	0.5 to 5	1	0.01 to 1
Parameter measured	Resistance	Voltage	Voltage or current	Resistance

Thermocouples work using the seebeck effect by measuring the voltage difference between two conducting materials that form an electrical junction. The voltage difference arise from the electromotive force developed by a temperature difference between the dissimilar materials and can be used to calculate temperature. Even though its working mechanism allows it to avoid the need of an external excitation, it is self powered, getting an accuracy in the range of decimals of a degree Celsius is difficult [3].

In the case of integrated circuits, they are semiconductor devices that use the current and temperature characteristics of a transistor. For example, voltage difference in the base-emitter of two transistors is proportional to their absolute temperature if operated at constant but different collector current [4]. Due to being mechanically delicate, they are more suited for embedded applications, inside equipment.

In both RTDs and thermistors, their resistance changes with temperature. In the case of RTDs, a metal, like platinum, nickel or copper, is used as the active material with a temperature dependent resistance (with a high temperature coefficient, resistance increases as temperature increases). With the thermistor, a semiconductor is used. The semiconductor's material can have either a positive or negative temperature coefficient (resistance increases as temperature increases with the positive coefficient and resistance decreases as temperature increases with the negative coefficient) [5].

1.1 Problem Background

As mentioned at the start of this section, temperature sensors are used in different industrial applications that require energy storage in fields like photovoltaic solar energy, electric power vehicles, grid electricity and power stations, etc. Battery, as a type of energy storage, is desired due to its capability of a fast transition, less than a second, from a standby state to a full power state when wanted.

In this sense, temperature sensors play a major role in assessing the condition of batteries as they would in any other electronic system.

Charge and discharge of a battery involve several stages that with appropriate monitoring and control can lead to getting the highest performance or efficiency of the battery, which is the role of a battery management system (BMS).

For example, in Li-Ion batteries, which are used in consumer electronics and electric vehicles, there are four stages in its charging phase [6][7], see figure 1.1.

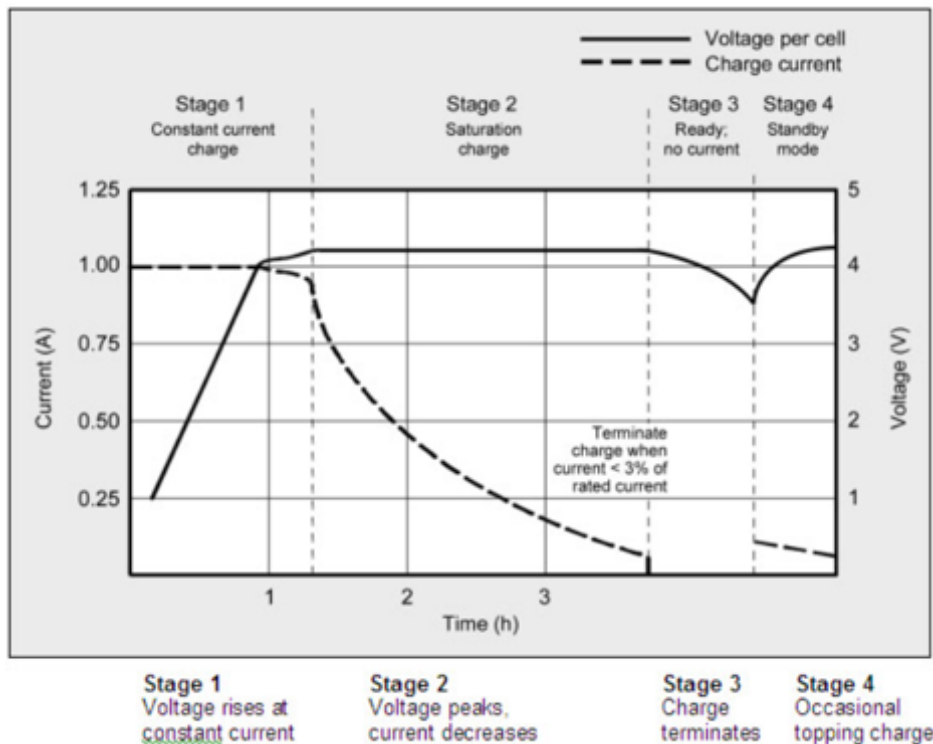


Figure 1.1: Charging stages in a Li-Ion battery [6][7].

The first stage is of pre-charge, where the voltage rises, at a constant current, to the value wanted. Second stage is of saturation, where the voltage is maintained constant while current decreases, here the battery is being charged. Once the current falls below 3%, battery has reached a fully charge state and the voltage is turned off, this is the ready stage. Finally, there is a topping charge stage when

the battery has been in a standby mode for a long period of time and the voltage has dropped and needs to be returned to its previous set value.

Controlling both voltage and current are linked to the battery's temperature. Having a temperature outside the wanted range in each stage can lead to a poor charge of the battery and can harm its life expectancy (a temperature below the wanted range leads to a slow charge and a too high temperature leads to a hazardous situation). As a consequence, special attention is wanted on the ambient temperature around the battery and on the increase of the battery's temperature during standard charging (around 5°C in Li-Ion batteries) or during fast charging scenarios where a certain temperature can not be exceeded without degrading the battery's performance.

Depending on the chemistry or composition of the battery, different acceptable working temperature ranges are needed. For example, in lithium cobalt oxide batteries, the upper temperature threshold is between 130 and 150°C before it reaches a dangerous situation, like an explosion. In lithium nickel manganese cobalt oxide, the threshold is between 170 and 180°C .

This implies the need for a refined control and monitoring, from the battery management system, on each battery cell's temperature condition in a pack. This can be achieved by having multiple temperature sensors mounted on the battery cell's body or electrical terminals, see figure 1.2

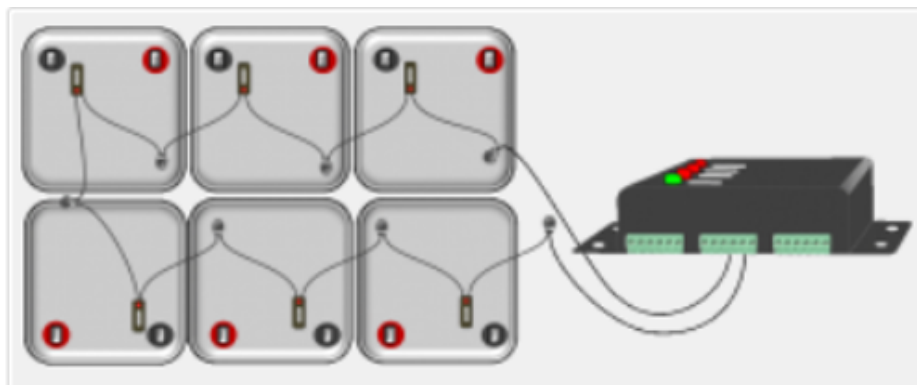


Figure 1.2: Monitoring of battery cell's condition through mounted temperature sensors [6].

As for the selection of a proper temperature sensor, it will depend on the application. In the case of batteries used for electrical vehicles, the general requirements for the sensor are the following:

- Temperature range from -40°C and 150°C .

- Flexible sensor that can be mounted and adjusted to the battery cell's surface.
- Accuracy between $\pm 0.1^{\circ}\text{C}$ to $\pm 0.5^{\circ}\text{C}$.

From table 1.1, it can be seen that a thermistor fulfills these requirements.

In the next section, the thermistor's characteristics and working principle will be further explained, specifically on negative temperature coefficient (NTC) thermistors. Furthermore, background on a solution from Holst Centre with its current issues will be shown. A possible optimization will be addressed as well, which is the aim of the present work.

2 NTC THERMISTOR

The characteristic behavior from a NTC thermistor can be traced back to 1833, when Michael Faraday noticed the resistance of silver sulphide decreasing as temperature was increasing. In the following century, a similar observation was made in transition-metal oxides like NiO . This followed several attempts to take advantage of this behavior and use it as a way to measure temperature. This includes a patent filed in 1930 from Samuel Ruben of a pyrometer device using copper oxide (Cu_2O) [8], an invention filed in 1935 from Walter Schottky as to the fabrication of a thermonegative resistor using a homogeneous ceramic (Cu_2O or UO_2) though there were some issue with stability due to the material's stoichiometry leading to changes in resistivity [9] and the influential research from Philips Research Laboratories in ceramic NTC thermistors (late 1940s) regarding spinel type structures and the properties related to the structure-composition. Further interest has been put since then to improve the stability of different ceramic and metal compositions (Cr_2O , $NiMn_2O_4$, $CuFe_2O_4$, $ZnMn_2$, for example), improve the temperature range as well as the accuracy [1][10].

2.1 Structure

Even though a NTC thermistor is not tied to a specific composition or ceramic family, the structure is centered on spinel types.

The spinel term is originally attributed to the structure of the mineral $MgAl_2O_4$ and similar minerals with the formulation of AB_2X_4 . This refers to X anions (like oxygen or other chalcogenides) arranged in a cubic or isometric lattice and cations A and B placed in tetrahedral and octahedral interstices, respectively, where the tetrahedra share corners with the octahedra and the octahedra share edges between each other. There are 8 AB_2X_4 units per unit cell, see figure 2.1. The distance between B cations is the shortest so it will determine the electrical conductivity. An inverted spinel would have the B cations in the tetrahedral sites and the A cations in the octahedral sites.

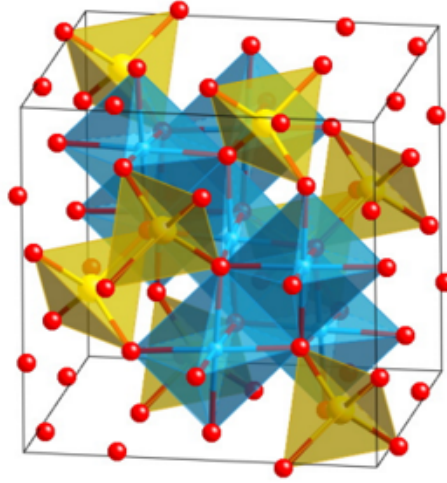


Figure 2.1: Spinel unit cell of the mineral $MgAl_2O_4$. Oxygen is in red, Aluminum is in blue and Magnesium is in yellow. The respective octrahedral and tetrahedral sites can be seen as well [11].

Apart from the spinel structure, there are others that have been studied: perovkites in the form of ABO_3 and pyrochlores in the form of $A_2^{III}B_2^{IV}O_7$. They will not be addressed as they are not part of the present work.

2.2 Characteristics

The two most important parameters of any NTC thermistor are its beta coefficient (B) and resistance at 25°C (R25). They come from the conduction mechanism within the NTC material.

As semiconductors form part of the composition, doping level determines the charge carrier concentration and it will not be affected by temperature; however, the charge carrier mobility will be as temperature will affect the number of electron-phonon collisions within the material. The temperature dependence of the resistivity can then be explained by the following Arrhenius equation:

$$\rho(T) = \frac{1}{\sigma} = \rho_{\infty} e^{\frac{E_a}{kT}} \quad (2.1)$$

Where $\rho(T)$ is the resistivity dependent on the temperature, σ is the conductivity, ρ_{∞} is the resistivity at infinite temperature or independent of temperature, E_a is the activation energy, T is the temperature and k is the Boltzmann's constant.

The activation energy is wanted in the range of 0.15 and 0.5 eV for the device to be useful as a temperature sensor [11]. This parameter can then be grouped with

the Boltzmann's constant as a characteristic of the ceramic material itself. In the case of ρ_∞ , it will be affected by the geometry of the thermistor. With this in mind, the previous formula can be expressed as:

$$R(T) = Ae^{\frac{B}{T}} \quad (2.2)$$

Where $R(T)$ is the resistance dependent on the temperature, A is the characteristic resistance of the material independent of the temperature and based on the fixed dimensions of the thermistor and B is the Beta coefficient of the material or its constant.

Beta coefficient can be found by measuring the resistance at two different temperatures. Normally, the temperatures chosen are 25°C (resistance measured at this point would be the R25 parameter) and 85°C, though different values can be chosen depending on the temperature range needed for the specific application. Calculation of the beta coefficient is then obtained from the slope of the 2 measured points (dividing the difference of the natural logarithm of the 2 measured resistance by the difference of the 2 inverse temperature values). This can be seen in the following formula:

$$\beta = \frac{\ln\left(\frac{R_{T1}}{R_{T2}}\right)}{\left(\frac{1}{T_1}\right) - \left(\frac{1}{T_2}\right)} \quad (2.3)$$

Where β is the beta coefficient, T_1 is the first temperature setting in Kelvin, T_2 is the second temperature setting in Kelvin, R_{T1} is the resistance at the first temperature setting in ohms and R_{T2} is the resistance at the second temperature setting in ohms.

In figure 2.2, it can be seen the R-T behaviour (resistance vs temperature) at different Beta values but with the R25 value (intersection of all the curves). Values from 2000 and 5000 K are common in the industry for sensing applications as values too low or too high can lead to little sensitivity to changes in temperature [1][12].

To summarize, tailoring the Beta coefficient (material composition) will affect the sensitivity of the thermistor while tailoring the R25, by fixing the geometry, will shift the curve to the temperature range wanted.

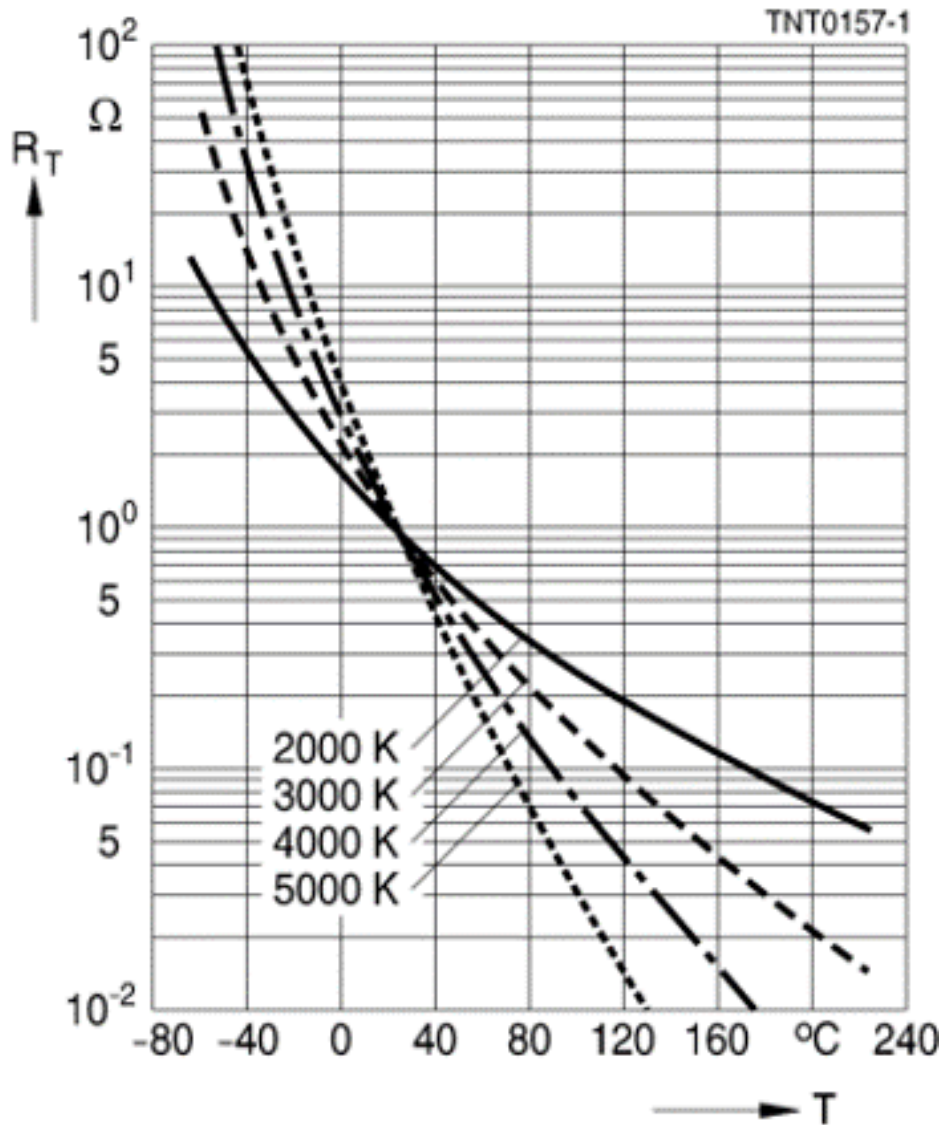


Figure 2.2: Resistance vs Temperature behavior in NTC thermistors at different Beta value coefficients [1].

2.3 Conduction mechanism

To finalize with the brief description of NTC thermistors, it is important to mention the conduction mechanism within the device. Since semiconductors are used as materials, the electrical flux happens from electrons moving inbetween ions. This is described as electron hopping mechanism, electrons attracting positive ions and repelling negative ions while moving through the lattice [11].

2.4 Holst Centre’s novel composite thermistor

In the previous section, it was mentioned the necessity for a flexible temperature sensor that could adapt to the topology of the battery cell’s surface and measure its temperature. For wearable applications, printed electronics are a suitable candidate as they have the mechanical properties needed while preserving the electrical characteristics within the requirements of the application. This is achieved through screen-printing or dispensing techniques on flexible substrates. Examples of flexible temperature sensors can be found in literature with focus on health monitoring [13][14].

Using a NTC ceramic sensor has the drawback of unsuitable mechanical properties, due to high stiffness, for flexible applications. However, a composite NTC ink, comprising the ceramic dispersed within a polymer matrix, printed on a flexible substrate is an optimal solution as the NTC ceramic provides the electrical properties, whereas, the polymer matrix or binder provides the mechanical properties.

Holst Centre developed a novel composite [15] that competes with industry’s current NTC temperature sensors [16] in terms of performance. It has a Beta coefficient of 3400 K and R25 of 100 $kohm$

The ceramic came from a manganese spinel oxide (ABO_4 type oxide), consistent of a mixture of Mn_2O_3 , NiO , Co_3O_4 , CuO and ZnO [17][18][19]. The material selected to act as matrix is a commercial binder precursor such as benzocyclobutene (cyclotene 3022-35 from Dow Chemicals).

2.4.1 Material processing and preparation

Due to confidential information, certain parameters are not shown but the overall process steps are still explained.

In terms of pre-processing of the material, the NTC ceramic or ceramic powder was obtained after being mixed on a roller bench for a day. For homogenization purposes, a dispermat bead mill with Zr marbles was used. Then, the material was placed in an oven overnight to dry. A mortar and pestle were used to break up agglomerates and the resulting powder was sieved through a 325-mesh sieve. For the activation of the ceramic, the powder was calcined in a high temperature air oven for 2 h and mixed again on the roller bench overnight. Moreover, the powder was mechanically pressed into pellets (40 mm wide) and sintered for 24 h and furnace cooled. Finally, the powder was obtained by grinding it with tungsten ball mill and sieved with a mesh of 45 um . Additionally, the sieved particles were passivated by submersion of particles overnight in a solution of phosphonic acid in

isopropanol. The particles were then vacuum filtered over filter paper and rinsed with isopropanol. The powder was then dried overnight in an oven. The particle size distribution of this material can be seen figure , as this same powder was used for the development of the present work.

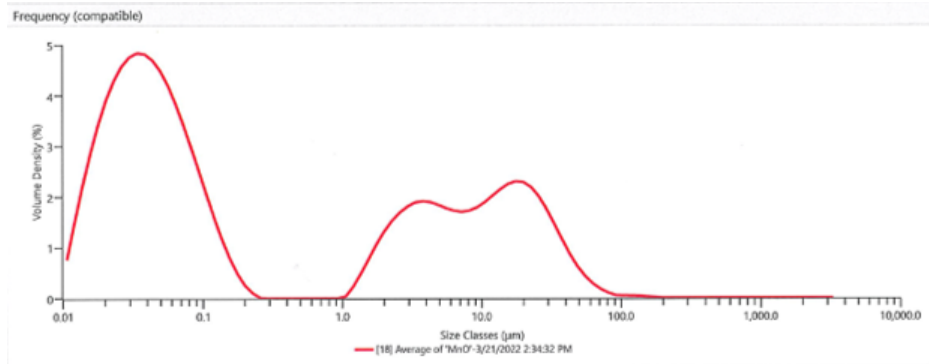


Figure 2.3: Particle size distribution of the ceramic powder.

Kapton sheets of 125 μm in thickness were chosen as flexible substrate. They passed through a pre-heating stage in an oven to compensate for shrinkage during the curing of the NTC ink, this will be further explained in the NTC ink mixture section.

Silver was chosen for the electrode material (DuPont 5025) so that it could be screen-printed on the substrate. Geometry followed a typical interdigitated (IDE) design. Thickness of the silver electrode is of 10 μm and its curing followed industry standards (120 °C for 10 minutes)

The binder had to go through a separate process before mixture with the ceramic powder as its solvent was not suitable for screen printing. Due to its low boiling point (165 °C) and high vapor pressure (2 $mmHg$), high shear rates from the effect of the squeegee on the ink as it is being pushed through the screen mesh can cause particles to aggregate faster and thicken the ink. Thus, reducing dramatically the "screen time" of the ink until it is too thick to be printed or uniformity of the film is not within the tolerances of the screen mesh anymore. To solve this issue, the solvent from the binder was evaporated through rotary evaporation and then replaced with 1-methylnaphthalene, that has a higher boiling point (244 °C).

The method to confirm that the 1-methylnaphthalene was adequate to replace the solvent in the cyclotene was through viscosity measurements of the final mixed ink at different shear rates (from 1-1000 1/s) every 15 minutes until 1 hour was reached. If initial viscosity is maintained in time in the range wanted, then it is safe to assume the ink is suitable for screen printing in that period of time (1 hour), though further understanding of the ink behavior for longer periods of

time was not studied. Furthermore, for the initial viscosity, a value within an order magnitude different of standard commercial silver inks for screen printing was looked for ($20 Pa.s$). Ink had a stable viscosity of $100 Pa.s$ for 1 hour.

2.4.2 NTC ink mixture

Mixture consisted of:

- Ceramic powder.
- Cyclotene without its solvent.
- 1-methylnaphthalene as the new solvent.

A planetary mixer was used for 2 minutes and at $2000 rpm$ to mix the components mentioned previously.

Curing of the NTC ink layer printed on top of the silver electrodes was done in steps due to the binder requirements. First it was done at $95\text{ }^{\circ}\text{C}$, followed by a step at $150\text{ }^{\circ}\text{C}$ and finally a curing step at $250\text{ }^{\circ}\text{C}$ in an oven. The NTC layer had a thickness of $45\text{ }\mu\text{m}$. On figure 2.4, a single printed NTC sensor can be seen.



Figure 2.4: Holst Centre's flexible NTC thermistor.

2.4.3 Issues

Even though Holst Centre's NTC composite proved to be suitable for screen-printing without compromising on the performance of the sensor, there are still some issues regarding the substrate used (kapton) and the sensor's behavior in extreme environmental conditions.

Curing temperature

As explained before, the binder used in the binary composite (cyclotene) has requirements regarding high temperatures needed for proper curing (up to $250\text{ }^{\circ}\text{C}$). PI substrates, like Kapton, are suitable materials for this temperature but are not desirable in the industry due to its cost and high water absorption. Choosing other substrates that can handle that temperature will not be a good solution

as the range of materials available is short and they will suffer from the same drawback, cost.

A polymer like PEN or PET would fit the market's needs better; however, the binder would need to be changed to allow a maximum curing temperature of 180 °C that will not affect the polymer.

Humidity stability

Resistance drift in time as well as humidity effect on the performance are some of the problems these type of printed NTC sensors can suffer from if they are not properly encapsulated or the formula has not been properly optimized.

A high humidity test was performed to address the impact of extreme environmental conditions on sensors without encapsulation. For this, a climatic chamber was used.

The sensors were connected to dataloggers outside of the chamber that registered the resistance of the sensors during the whole test, see figure 2.5. The climatic chamber cycle consisted of a varying relative humidity from 50% to 85% and then back to 50% every 100 hours. Temperature oscillated between 20 °C and 60 °C every 5 hours. The whole cycle lasted 300 hours (12 days).



Figure 2.5: Climatic chamber setup for high humidity test.

Results from the test can be seen in figure 2.6. Normalized resistance values are shown in red and blue (for 2 types of Holst Centre's NTC ink) but in both of them

the behavior is the same. After the first humidity cycle (in black), the resistance does not go back to its initial value. There is a shift around 8% in the resistance value. This shift keeps happening in following humidity cycles. Furthermore, the resistance seems to follow the humidity (resistance increases as humidity increase and resistance decreases as humidity decreases) in each cycle even though the temperature (in green) does not. This change in resistance from the influence of humidity but not from temperature can lead to the reporting of a different measured temperature from the thermistor (an offset of even 1 °C would already fall out of the accuracy expected from these types of sensors).

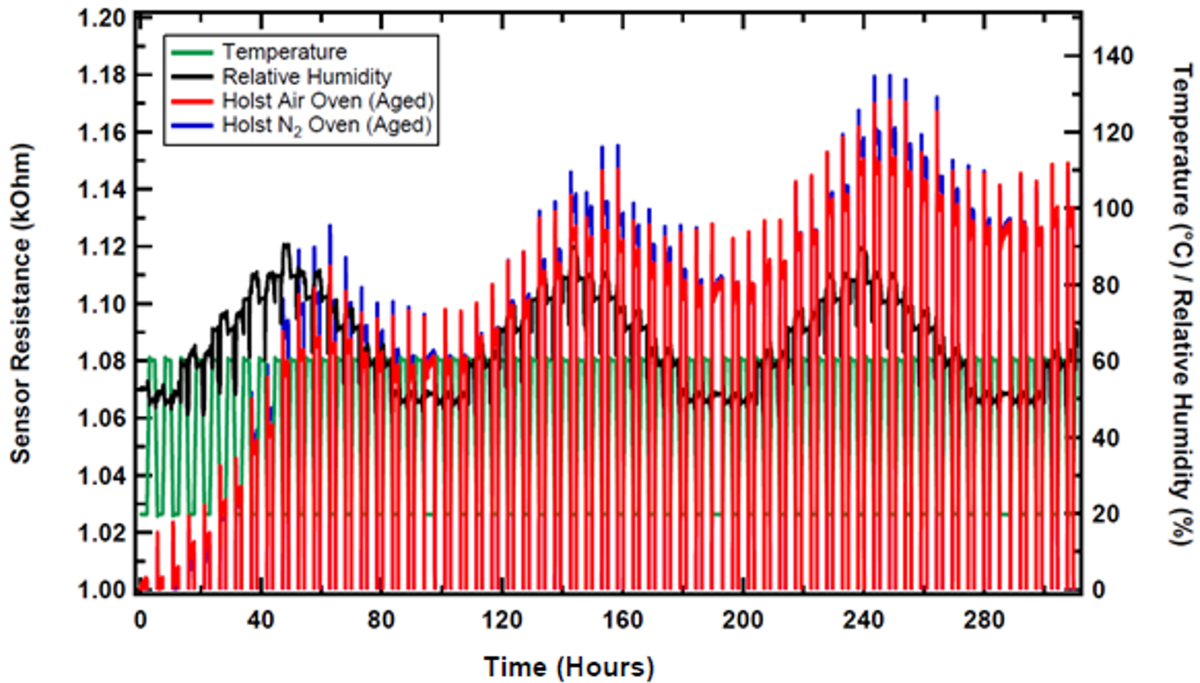


Figure 2.6: NTC composite response at a continuous change of temperature and humidity for 12 days [20].

Even though the cyclotene selected for the current NTC formula has hydrophobic properties, using Kapton as a substrate (because of the high curing temperature conditions) has the opposite effect. Furthermore, the material used for the electrodes (silver) is an active metal that can react in harsh environmental conditions. All these factors could have contributed to the behavior seen in figure 2.6 but it is important to understand which factor in contributing the most.

Several encapsulation methods were also tested like the use of lamination between glasses or by printing barrier layers used for solar cells [21]. Humidity effect improved but still the change in resistance compromised the sensor’s performance.

2.5 Epoxy-ceramic based NTC thermistor

Changing the binder could help tackle both of the issues explained before. An epoxy based binder is a suitable candidate due to its low curing temperature (below 200 °C) and because it can also act as a humidity barrier (this has been widely used in the industry in encapsulation applications).

One epoxy was selected from a supplier's catalogue as it complied with what was explained in the previous paragraph. The curing process consist of putting the sample at 150 °C for 30 minutes and then increased the temperature up to 180 °C and hold it for 1 hour. Ideally, a maximum curing temperature of 150 °C would be preferred to have wide range of available substrates but some PEN and PET foils can handle a temperature of 180 °C so it is still suitable for the current application.

Main components of the epoxy cannot be disclosed but consist of:

- Resin A.
- Resin B.
- Hardener.
- Solvent.

Amount for each component follows the recommendation of the supplier and they are mixed in the planetary mixer for 1 minute at 2000 *rpm* (enough time for deaeration).

2.6 Research questions for an epoxy-ceramic based NTC temperature sensor

Both the problem and possible optimization path has been stated so far. In this sense, the aim of the present work is to understand 2 topics in the epoxy-ceramic NTC thermistor solution:

- Investigate the effects of the amount of ceramic vol% in the NTC ink mixture, the effect on the electrical properties from external pressure applied on the sensor, the effect of electrode geometry on the epoxy-ceramic composite.
- Understand the effect of humidity on an epoxy based solution as well as the role of electrode material and how much it contributes to the humidity dependence of the NTC ink.

In the next sections, methods to assess the previous questions will be explained,

results from the tests will be presented and a discussion of the results and conclusions drawn will be shown.

3 METHODS

Before going into the different tests planned for the epoxy formulation, it is important to discuss the procedure done to prepare each sample and how it was characterized/calibrated before and after every test.

In figure 3.1, there is an overview of the steps followed to prepared the NTC samples and characterize them.

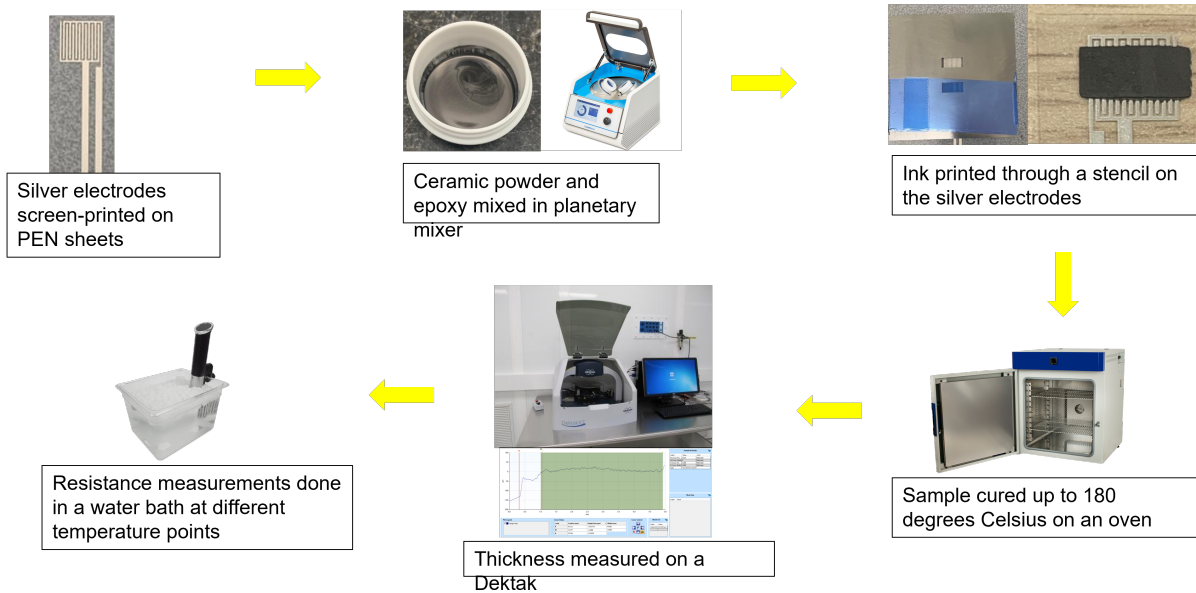


Figure 3.1: Overview of sample preparation and characterization.

Silver electrodes were first screen-printed on PEN sheets that can withstand a temperature of up to 180 °C (Q65HA [22]). Silver material was the same used for Holst Centre’s flexible NTC thermistor (Dupont 5025). A 10 *um* layer with an IDE design was printed and cured at 120 °C for 10 minutes.

For the epoxy-ceramic mixture, an analytical balance from Waagenet with a precision of 0.0001 *g* was used to make sure the amount per component stays the same or as close as possible every time a sample is prepared. Since only a couple

samples are prepared at a time, 1 g of ink is mixed every time. A planetary mixer was used for the mixture, settings were 2 minutes at 2000 rpm.

To apply the ink on the silver electrodes, screen-printing is not possible as a new screen mesh would need to be prepared every time there is a change in design. Stencil-printing was selected, using a stainless steel foil (150 μm in thickness) and blade as a squeegee tool (even though mylar is commonly used as a material for the stencil, stainless steel is preferred so as to avoid reactions with the solvents used for cleaning). Curing of the samples is then done in an oven.

For the characterization, since the stencil-printing is done manually, thickness of the samples has to be measured as there is no tolerance from the printing process. Dektak is used for this purpose and the average value of a section of the profile is taken, see figure 3.2.

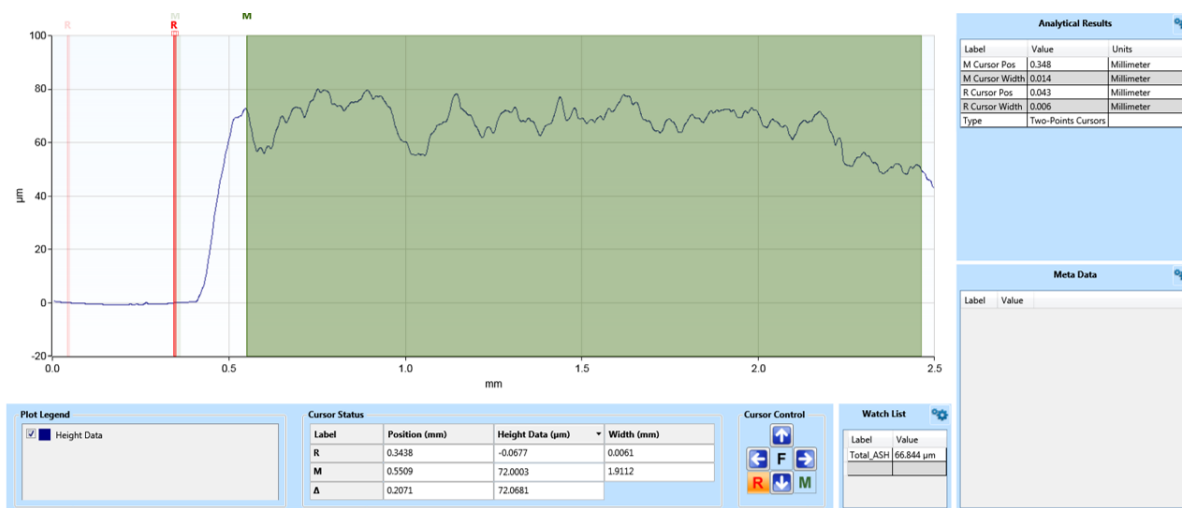


Figure 3.2: Thickness measurement of a NTC sample on the electrode region using Dektak.

Finally, to characterize the electrical properties of the sensor, resistance should be measured at two temperature points (see equation 2.3 for calculation of the Beta coefficient). Accuracy of the temperature settings is important so a water bath was chosen since it is easier for temperature to be kept homogeneously in a fluid. The heater used to control the water temperature is the Anova AN400-20 which has a temperature accuracy of ± 0.1 $^{\circ}\text{C}$. Samples are put inside a plastic bag and then submerged in the water bath, leaving the connection leads outside for resistance measurement with a multimeter.

Resistance of the samples are linked to its geometry, which is why thickness is measured in every sample. In this sense, instead of comparing the resistance values from the multimeter between each sample, volume resistivity should be

taken into account to get rid of the thickness difference between samples. This resistivity is calculated as the following [23][24]:

$$\rho_v = R_v \frac{A}{T} \quad (3.1)$$

Where ρ_v is the volume resistivity in $ohm.cm$, R_v is the volume resistance measured by the multimeter, A is the area of the electrode and T is the thickness of the electrode.

For the area calculation, even though the NTC ink is printed to cover completely the width of the IDE shape, only the region in between the silver electrodes will contribute to the performance of the thermistor [25]. Find this area is easy as the dimensions of the IDE and stencil printing area are known (fingers of $300 \mu m$ in width and distance of $300 \mu m$ between electrodes), see figure 3.3.

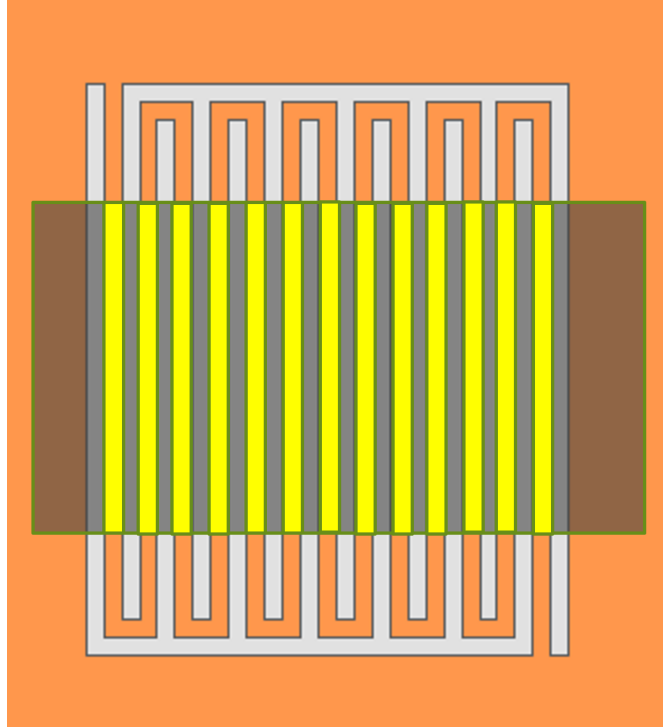


Figure 3.3: IDE electrodes in gray with the NTC ink printed on top (dark area). In yellow is shown the active region that contributes to the functioning of the thermistor and from where the area, for resistivity calculation, is taken from.

3.1 Functional granular composites

The weight ratio for the ceramic powder, cyclotene and solvent mentioned in NTC ink mixture section, was obtained through iterations and part of a research before

the start of the present work. A more systematic process was approached for the new binder to avoid several tests. Literature on functional granular composites (FGC) was looked into in order to understand how the mechanical properties of polymers combine with the electrical properties of the ceramic [11][26][27].

FGC can be divided by the degree of connectivity between the two or more components in the composite. Physical properties may change depending on how the components are connected, so special attention should be put if there is a specific characteristic that should be maintained. The degree of connectivity can be described with a 2 digit syntax in which the first one is related to the connectivity of the ceramic and the second one to the connectivity of the polymer binder (or epoxy matrix in the case of the present work). The syntax value refers to how many dimension is connected to, see figure 3.4 (thinking of 3 dimensions or axis relates to properties like conductivity or permittivity).

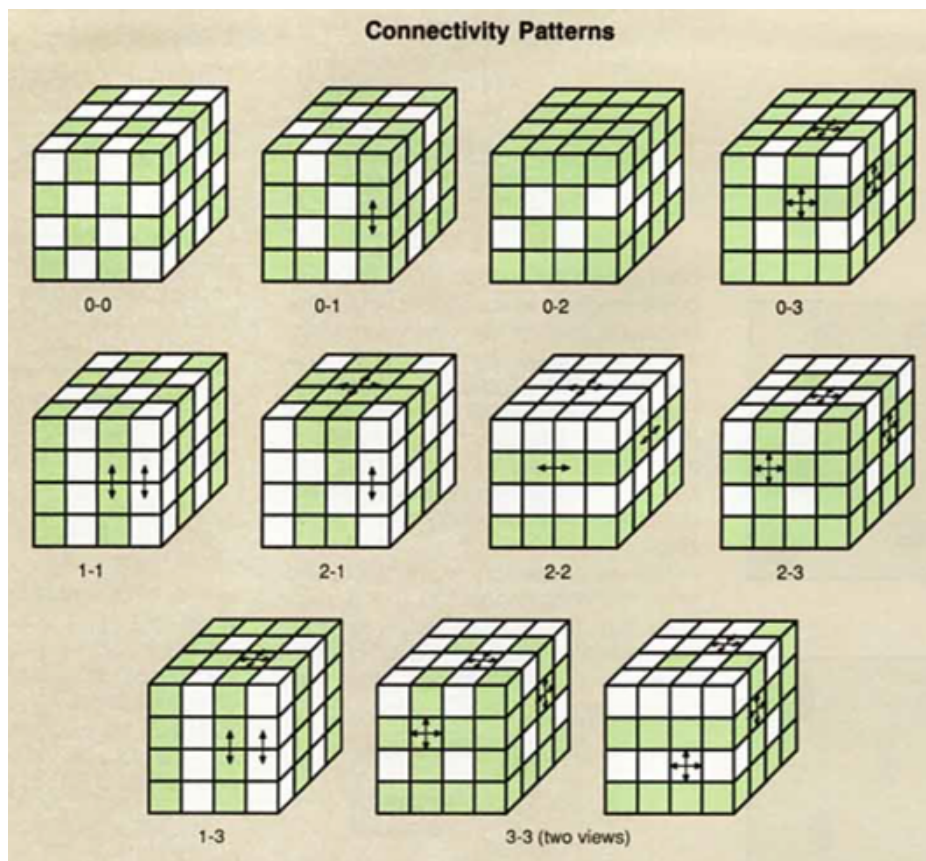


Figure 3.4: Syntax of connectivity between components in functional granular composites.

0-3 composites are the easiest to produce as the dispersion of the ceramic particles within the polymer matrix is done randomly; however, this leads to low connectivity of the ceramic and limits the functional properties of the composite.

1-3 composites, on the other hand, have a ceramic connectivity in at least one dimension or in columns, which leads to easier conduction paths and easier access to the functional properties of the particles.

As connectivity increases, so does the functional properties. 3-3 composites represent the best 3D connectivity. At the same time, achieving greater connectivity involves more complex processes.

If a 1-3 composite is wanted, it could be achieved by structuring via dielectrophoresis (DEP); however, due to equipment limitations during the present work and the mixture process explained previously (use of planetary mixer for dispersing the ceramic particles in the epoxy matrix), the composite 0-3 will be kept for the following tests.

In this sense, to overcome the disadvantages of a 0-3 structure (low particle connectivity), the proper volume ratio between the ceramic particles and the epoxy matrix must be found.

Having a larger volume of the binder in the mixture would mean better mechanical properties of the ink as it will become more flexible easier to apply through screen printing. However, less ceramic volume content also means the overall resistance of the composite will increase. On the hand, increasing the ceramic content helps with conductivity and better electrical performance but it also means the ink will become more brittle and, as a consequence, lead to a loss of connection between electrodes from constant use. A trade-off in the electromechanical properties is needed when adjusting the proper volume ratio between the ceramic powder and the epoxy binder.

The minimum amount needed before loss of the ceramics functional properties is know as the percolation limit or critical volume, see figure 3.5. Knowing this limit will help understand at which volume the conduction paths formed within the ink are good enough for proper connectivity between the electrodes in the NTC sensor.

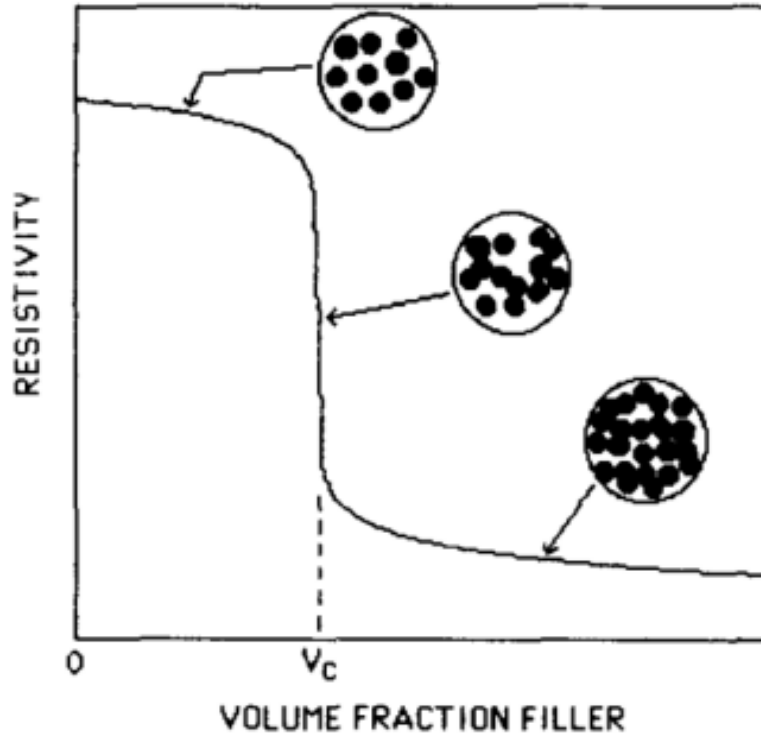


Figure 3.5: Percolation limit or critical volume in a functional binary composite.

5 different volume ratios were prepared to find the percolation limit of the mixture. The ceramic volume contents were: 50 %, 40 %, 35 %, 30 % and 20 %. SEM pictures were taken to verify if cluster or agglomerates of the ceramic powder forms at higher volume fractions as well as the distance between particles and understand why a characteristic like resistance would change depending on the amount of ceramic volume in the mixture.

3.1.1 Composite model

One way to understand the degree of connectivity is through the Lichtenecker model. It is based on Wiener's theory about the lower and upper limits of a specific property in a composite consisting of 2 phases [28]. Even though in the referred literature, the model is used for the effective dielectric function, it can be adapted to other properties like conductivity [11].

The upper and lower limits for resistivity (or conductivity) in a binary composite can be associated to the parallel and series addition models, see figure 3.6.

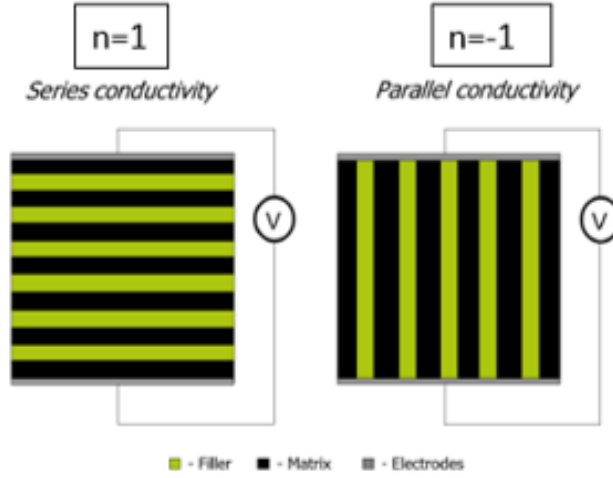


Figure 3.6: Upper limit (represented by factor $n=1$) and lower limit (represented by factor $n=-1$) in resistivity in the form of ideal series and parallel connectivity, respectively, in a binary composite [11].

In these approximation, the series connectivity assumes the filler (ceramic component in green) and matrix (epoxy component in black) are stacked in layers, interleaved, in between the electrodes in grey. This represents the worst possible connectivity between the two components at every ceramic volume fraction in the composite. This can be represented by a factor n with an upper limit of 1.

The parallel connectivity assumes the filler and matrix are stacked vertically, with the filler having direct connection to the top and bottom electrodes. This represents the best possible connectivity between the two components at every ceramic volume fraction in the composite. This can be represented by a factor n with a lower limit of -1.

To properly model this two extreme scenarios, and any others in between, the following formula can be used (which uses the Lichtenecker's rule as how to bridge a series connectivity and a parallel connectivity in a binary composite):

$$\rho_c^n = \varphi \rho_{NTC}^n + (1 - \varphi) \rho_p^n \quad (3.2)$$

Where ρ_c is the resistivity of the composite in $ohm.cm$, φ is the volume fraction of the ceramic, ρ_{NTC} is the resistivity of the ceramic in $ohm.cm$ (value is 20 000 from Holst Centre's previous work), ρ_p is the resistivity of the matrix or polymer in $ohm.cm$ (value is $1E+11$ from supplier) and n is a factor that can go from -1 (parallel scenario) to +1 (series scenario)

This model was plotted with the resistivity values taken from the samples at 5

different volume ratios to understand in which type of connectivity the mixture was at.

3.2 Particle-to-particle contact

Once the optimal volume ratio between the ceramic powder and the epoxy has been defined, it is important to further understand the influence of the mixture in the overall resistance of the ink and understand how can the conductivity be improved (depending on the application of the temperature sensor).

Even though the electrical properties are dependent on the ceramic properties, the conductivity will be affected as well by how the conduction paths between particles were formed within the binder matrix.

In this sense, the overall resistance will depend on the composite resistance, electrodes resistance, particle-to-particle resistance, resistance across one particle, the number of particles in a conduction path and the number of paths in the mixture.

From the resistances mentioned in the previous paragraph, most of them can be simplified by assuming a cubic packaging in the composite (particles per path and number of paths can be assumed by geometry factors; electrode and particle resistances are dependent on the raw material) leaving the particle-to-particle resistance as the main contributor to the NTC ink electrical properties.

The particle-to-particle resistance can be further divided into 3 factors which will be briefly analyzed in the following sections.

3.2.1 Constriction resistance

As 2 particles come into contact to form the conduction path, only a section of the surface of the sphere that touches the other sphere allows the flow of electricity even though the whole sphere surface is capable of doing it and, as a consequence, there is a loss of energy in the form of resistance.

The constricted flow of electricity can be explained from the decreased diameter dimension available when 2 particles are in contact, see figure 3.7.

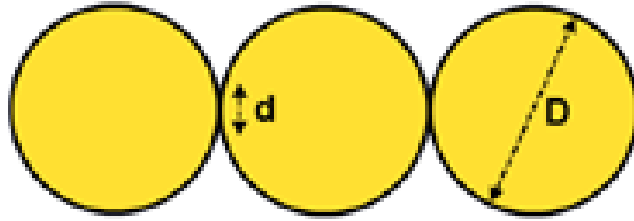


Figure 3.7: Constriction resistance [11].

By controlling the size of the particles, the influence of this resistance can be reduced but the size is already defined in the available raw material as part of the pre-processing, see figure 2.3. Tests on how to improve this resistance will not be part of the present work.

3.2.2 Tunneling resistance

In the previous section, the physical contact between 2 particles was mentioned. However, in reality, each particle will have an insulating layer around its surface that must be overcome before flow of electricity can take place, see figure 3.8. This can be due to the ceramic powder being an active material that when exposed in an air environment can oxidize to some degree. Moreover, residues during the pre-processing of the powder could also explain the insulating film around the particle. Finally, the binder itself can as well insulate the conductive spheres.

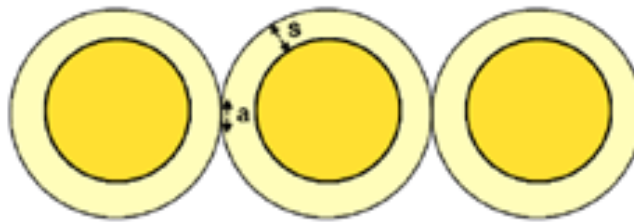


Figure 3.8: Tunneling resistance [11].

Even though the presence of this insulating layer influences the overall resistance, the effect can be ignored as only a thick layer could avoid electron tunneling to take place. Tests on how to improve this resistance will not be part of the present work.

3.2.3 Deformation dependent resistance

In the constriction resistance section, the influence of the contact area between 2 particles was explained. However, if there is a force, or a pressure, applied to

the particles and they are pushed together, then the contact area increases and the conductivity can improve. On the other hand, if the force instead pulls the particles apart, the contact area decreases, or even breaks, and the conductivity can decrease, see figure 3.9.

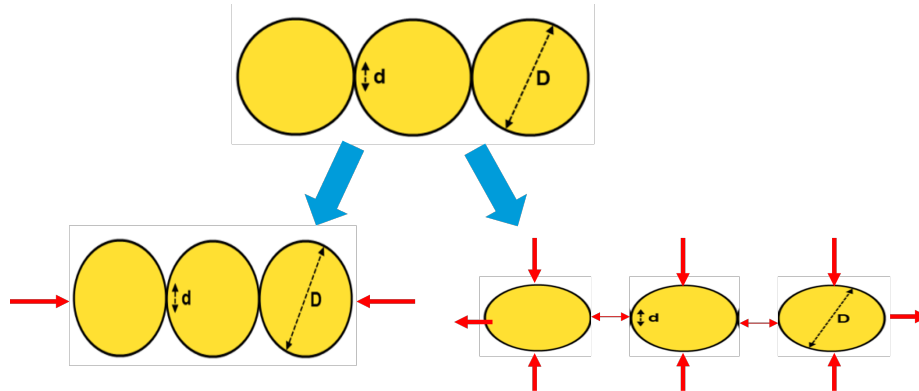


Figure 3.9: Scenario on the bottom left shows particles being pushed together because of an external force/pressure. Scenario on the bottom right shows particles being pulled apart because of an external force/pressure.

In this sense, a test with applied pressure on 2 samples was performed to assess which of the two scenarios is more likely to occur when an external pressure is applied to the NTC thermistor (for example, when the sensor is mounted on the battery cell's body).

This was done with the aid of a thermal bonding device that can apply a pressure up to 0.55 MPa . The equipment is calibrated with a loading cell so that a relation between pressure and force can be established, see figure 3.10.

For each sample, different pressure values were applied until the maximum was reached (every 0.1 MPa), resistance was measured after each pressure and resistivity was calculated and plotted.

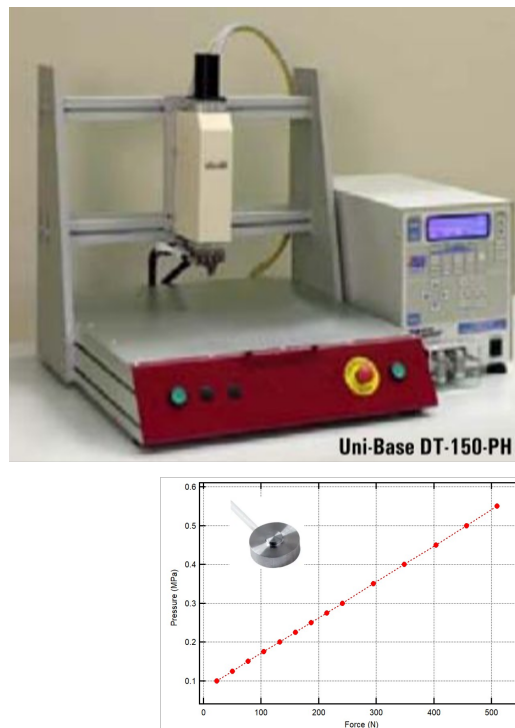


Figure 3.10: Thermal bonding device.

SEM pictures were taken before and after the test to verify if the distance between particles decreased or increased from the pressure applied and correlate them with the resistance measurements.

3.3 Electrode geometry effect on resistivity and connectivity of the NTC temperature sensor

In [29], the influence of the electric field in the electrode design was analyzed. Knowing that the resistance is linked to grain and grain boundary within the ink, the thicker the NTC ink gets, the more the grain boundary resistance becomes dependent on the distribution and intensity of the electric field applied to the electrodes. Furthermore, since electron hopping conduction is the main type of conduction within the NTC sensor (seen in NTC thermistor section), a higher electric field effect could help improve the electron mobility and thus reduce the overall resistance and improve the linearity in the R-T behavior of the sensor.

To test whether the electric field can be used as another way to improve the electrical properties of the sensor, simulations on Ansys were performed. Different geometries were looked at in order to understand how can the electric field distribution could be improved while maintaining the same electrode width and distance between electrodes in every design (300 μm). 8 configurations with ex-

pected different influence on the electric field were reached, see figure 3.11. To properly compare the results of each design, only the active region is taken into account and volume resistivity is calculated.

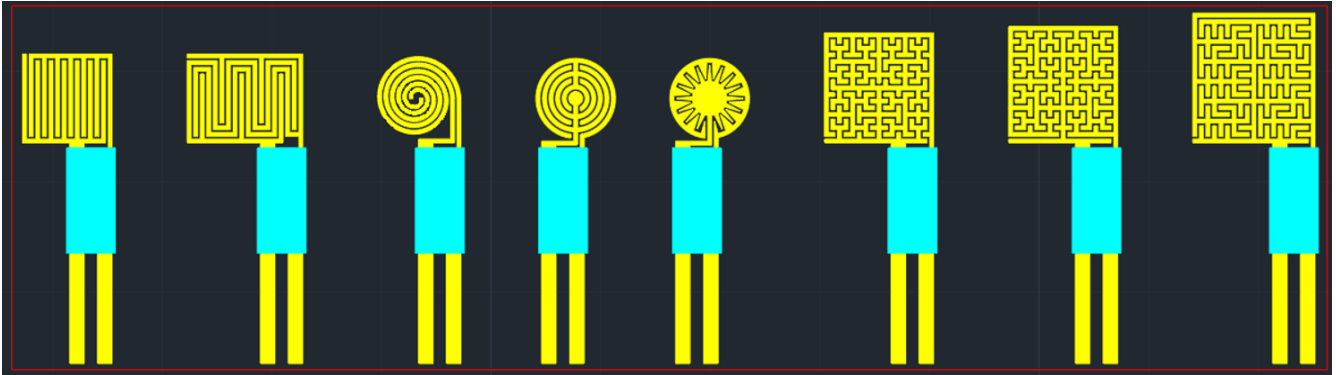


Figure 3.11: Electrode geometries. From left to right, IDE electrode design, serpentine design, spiral design, concentric design, spike design, fractal Hilbert design, fractal Moore design and fractal Peano design.

The IDE design is taken from Holst Centre’s design as it will be used as reference for the other designs. This finger-type geometry is typically used in printed thermistors as you can have a bigger active region between the electrodes than you would have with planar electrodes in the same area [30][31][32].

The serpentine design have been used for applications where a higher capacitance, from a larger active region, than the standard IDE could be achieved (applications related to capacitive sensors) [33][34][35].

The spiral design is used as well in some temperature sensors [33]. Though the active region may be larger than the IDE one, it is expected that the electric field will not have a stronger distribution on certain sections as the whole geometry is uniform (different from the finger-tip sections in the two previous designs).

The concentric (or ring-shaped) and spike (or radial) design were taken into consideration as they have been studied for applications regarding ER effect (electrorheological effect, change of viscosity in response to an applied electric field) where the impact of the geometry of the electrodes with the electric field was assessed [36]. Furthermore, they were also studied in electrochemical capacitive applications [35][37].

Fractal designs have been studied for use in microcapacitors. Typically an IDE design is used but findings show that fractal shapes are desirable due to a larger active region for an enhanced electrochemical performance and lower energy loss in ion-transport (higher energy density). These shapes have a larger amount of

open and rough edges that have better edging effect (lateral electrical flux) when compared to the fingers of the IDE design [38], see figure 3.12. For fractal Hilbert, Moore and Peano; the concept is of a continuous fractal space-filling curve in a specific region.

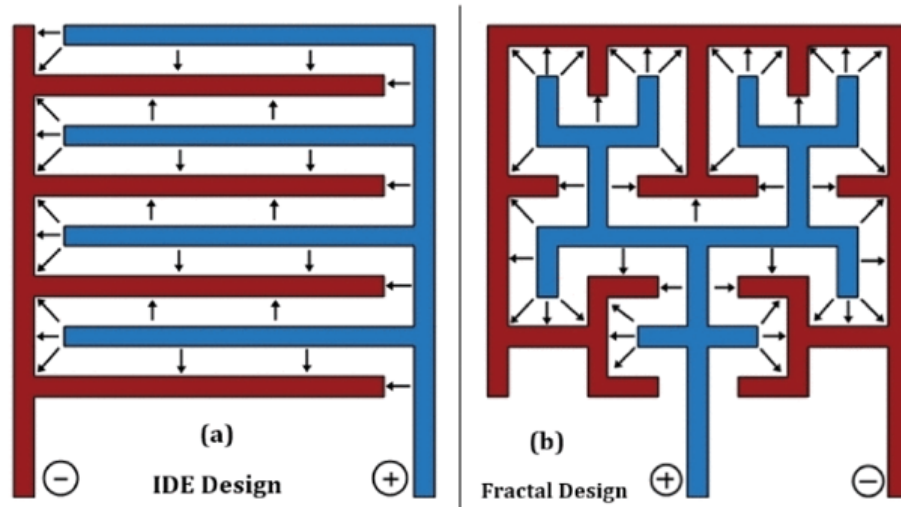


Figure 3.12: Comparison between IDE and fractal design with electrical lines at the edges [38].

For the simulations, Maxwell equations were used with a voltage applied of 10 V. Silver electrodes were simulated on top of a PI substrate. A vacuum box covering all the elements was also used to minimize influence of the atmosphere.

3 samples of each design were then prepared and connected to a source meter (Keithly 2610A) so that voltage from 1 to 10 V could be applied. Resistance was measured every 1 V and resistivity was calculated for comparison between designs (active region is different in each design so this was also taken into account for the resistivity calculation).

3.4 Humidity stability

As mentioned previously, one of the advantages of using epoxy in the NTC formulation is that it has some encapsulation properties and could potentially act as a humidity barrier.

To verify this, 3 samples were prepared and put in a climatic chamber for testing. The cycle used can be seen in figure 3.13. The humidity cycle (in red) goes from 50 RH% up to 90 RH% and then returns back to 50 RH%, in steps of 10 RH%. The temperature cycle (in green) goes from 20 °C up to 60 °C and then returns back to 20 °C. The climatic chamber is set so that 2 temperature cycles happen for each

humidity step. Duration for the complete test is of approximately 100 hours (or 4 days). Resistance of the samples is measured during the whole test with the aid of dataloggers outside the climatic chamber (same setup used for Holst Centre's NTC thermistor humidity test).

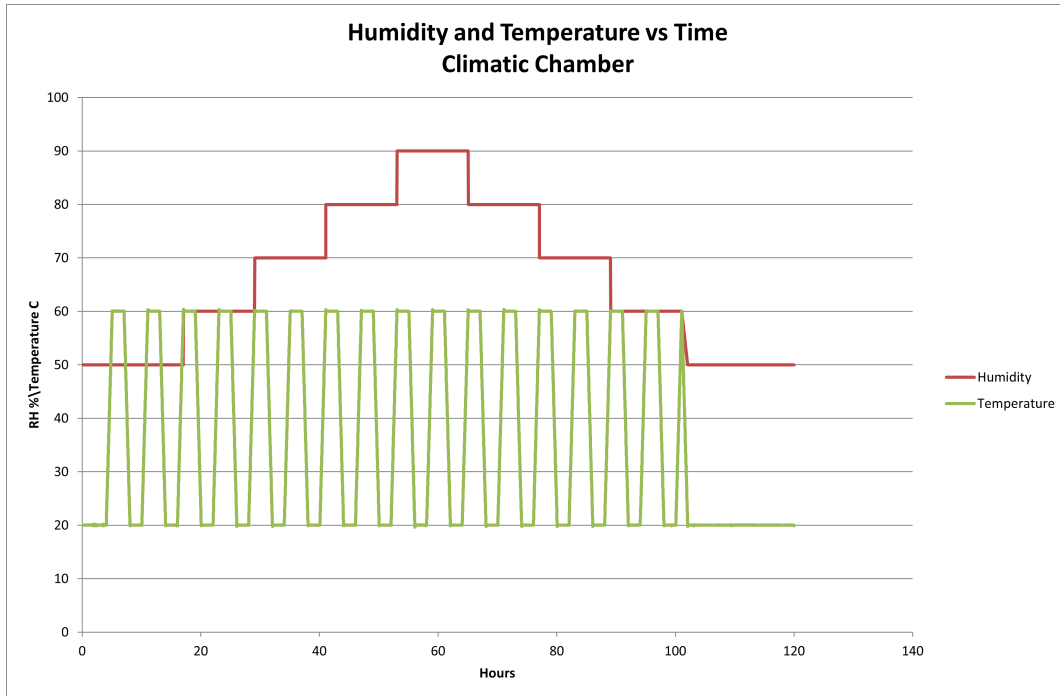


Figure 3.13: Climatic chamber settings for high humidity test.

Additionally, to assess the influence of a high humidity environment on the electrode material, 3 more samples were prepared, but with nickel-gold coating for the electrode, to be put in the climatic test as well, see figure 3.14.

The rationality behind this is that gold has better corrosion resistance and wear resistance (when alloyed with nickel) than silver with still high electrical conductivity (though lower than the silver's one) [39]. Being an inert metal, it can be expected that the effect of a high humidity environment on the electrode will be much lower as it is not an "active" material like the silver electrodes are.

By keeping the same electrode shape and NTC formulation (with the optimal volume ratio of the ceramic and epoxy already found), it can be properly compared with the silver samples and understand the effect from the electrode material in humidity stability.

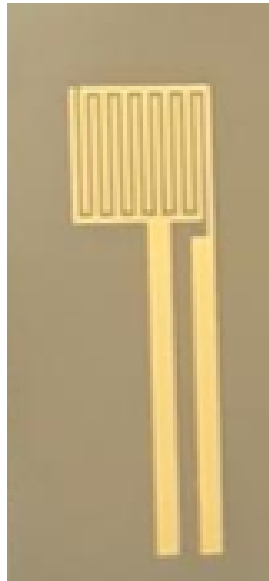


Figure 3.14: IDE electrode printed on a PI substrate and with a nickel-gold coating.

4 RESULTS

4.1 Percolation limit

On figures 4.1 and 4.2, the resistivity and Beta coefficient, respectively, at different ceramic volumes can be seen. A stable low resistivity is achieved in the range of 40 to 50 % ceramic volume concentration. For lower concentrations, resistivity increases rapidly which means the composite is losing the electrical properties from the ceramic powder and gaining more properties from the epoxy matrix. In the case of the Beta coefficients, a stable 3400K is maintained in the range of 35 to 50 % ceramic volume concentration. Similarly, for lower concentrations, there is a rapid decrease. It should be noted that for the rest of the tests, formulation was kept at 40 % of the ceramic volume.

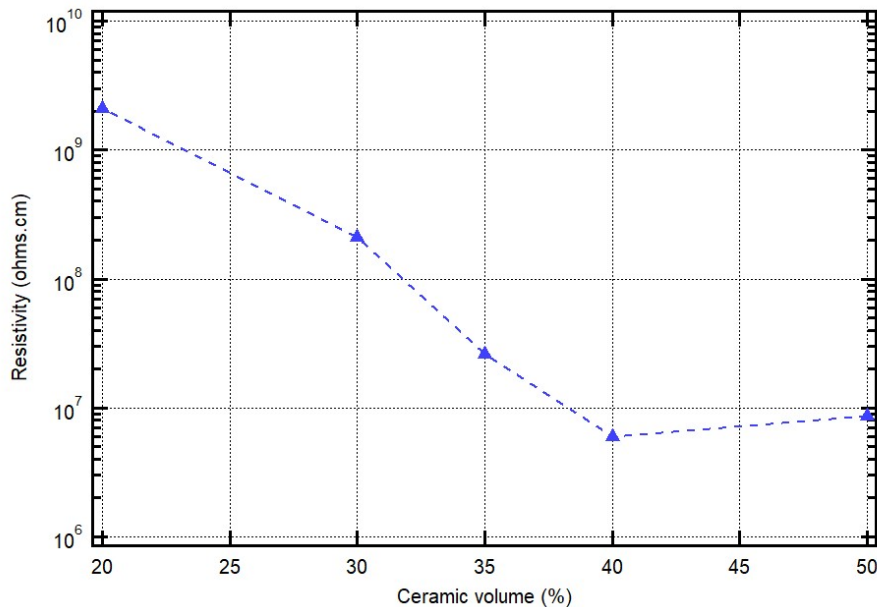


Figure 4.1: Resistivity at different ceramic volumes (20 %, 30 %, 35 %, 40 % and 50 %).

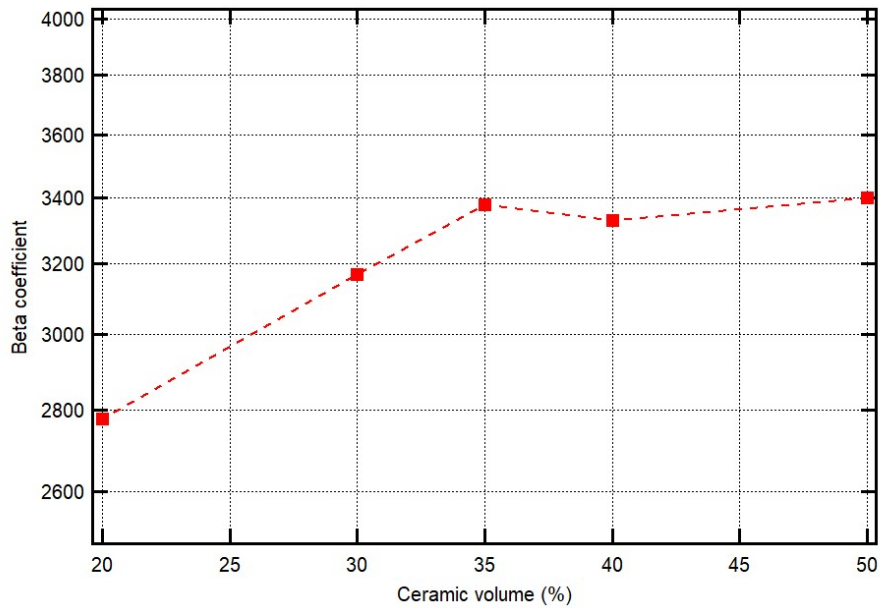


Figure 4.2: Beta coefficient at different ceramic volumes (20 %, 30 %, 35 %, 40 % and 50 %).

On figure 4.3, the Lichteneker model is used to understand the degree of connectivity of the samples. At 40 %, the n factor is of -0.1 approximately which shows that the NTC mixture is not close to the best possible connection (parallel connection or $n=-1$) nor in the worst possible connection (series connection or $n=1$).

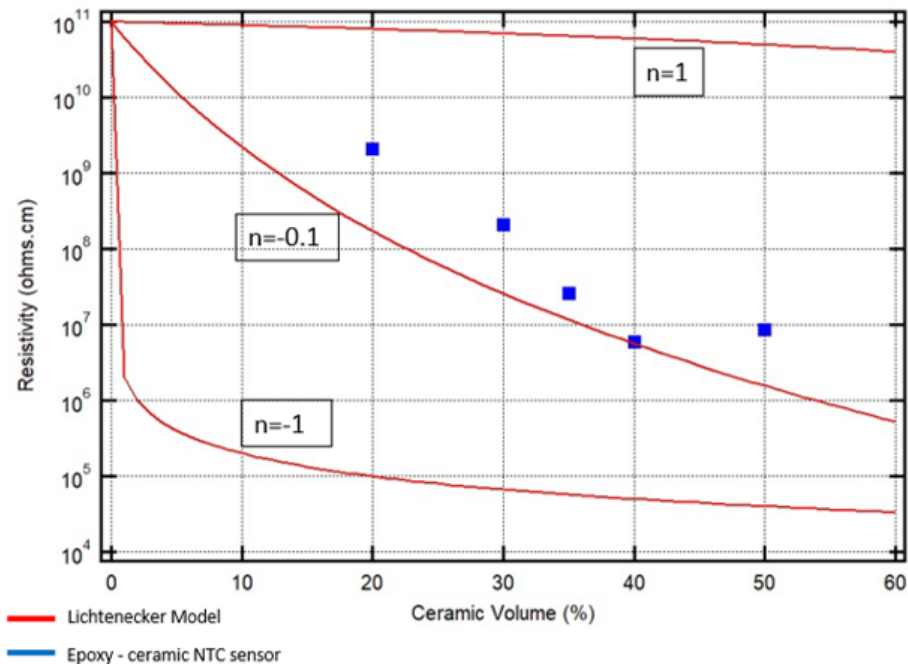


Figure 4.3: Lichteneker model fit with resistivity at different ceramic volumes.

In figure 4.4, the SEM pictures at every ceramic volume percentage tested are

shown. From the EDS analysis, the epoxy (red region from carbon atoms) and the NTC ceramic (green region from manganese atoms) can be distinguished more easily. Additionally, it can be seen clearly that larger concentrations (40 to 50 %) present more aggregates of the ceramic particles forming conduction paths than in the lower concentrations, which are mainly isolated islands of the ceramic particles (explaining the behaviour of resistivity vs ceramic volume concentration).

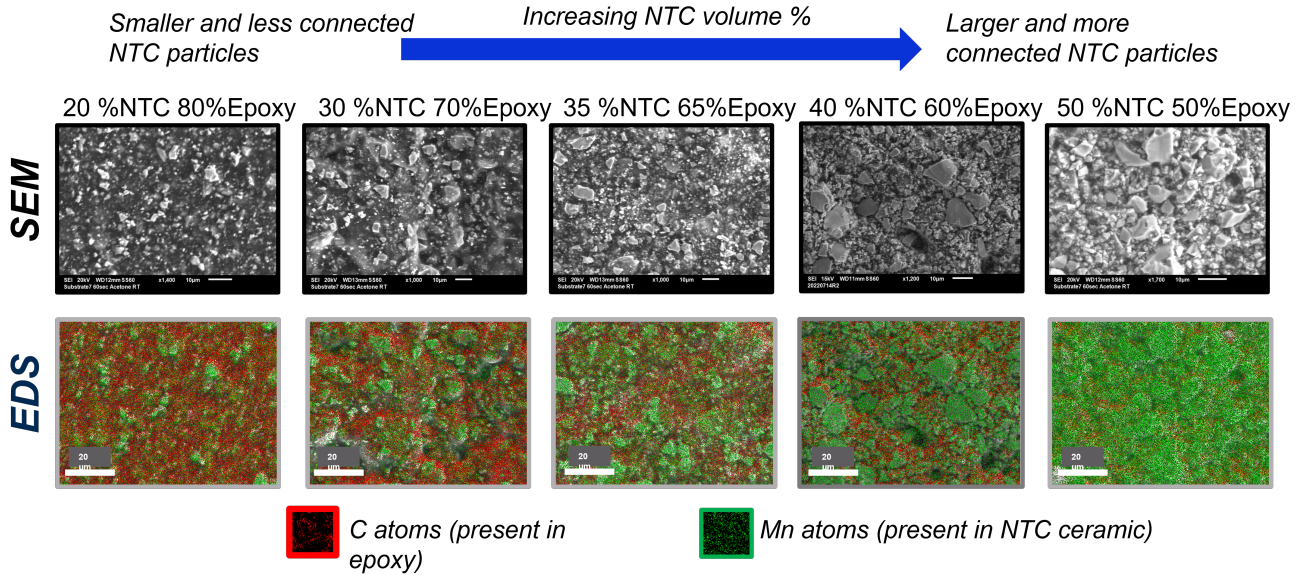


Figure 4.4: SEM pictures and EDS analysis of NTC samples in the electrode region at 5 ceramic volume concentrations.

4.2 Pressure influence

From figures 4.5 and 4.6, it can be seen that resistivity consistently increases with the amount of pressure applied to the samples and the change is irreversible. The SEM pictures with the EDS analysis shows that pressure has broken some of the conduction paths formed before any pressure was applied and has isolated some clusters of ceramic particle within the composite, which explains the increase in resistivity.

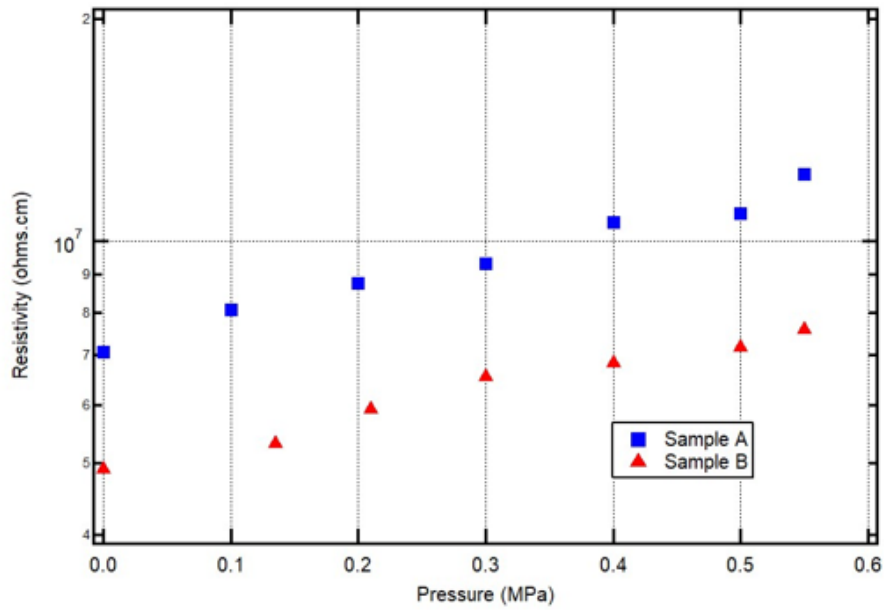
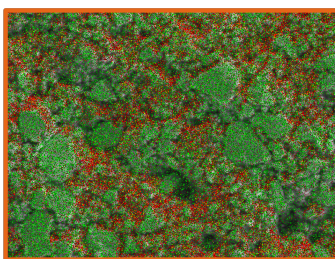
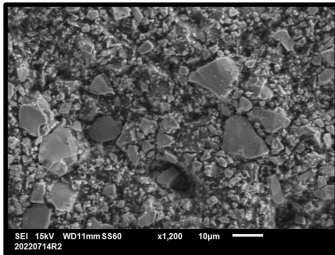


Figure 4.5: Resistivity of 2 samples with an external pressure applied.

Before Pressure (0 MPa)

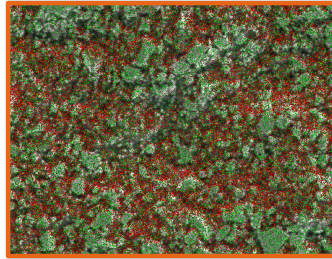
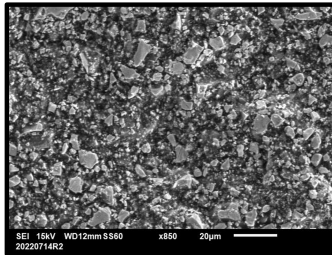
Larger NTC particles, more interconnectivity



Resistivity =
7.07e+06

After Pressure (0.55 MPa)

Smaller NTC particles, less interconnectivity



Resistivity =
1.23e+07

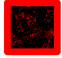
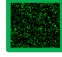
 C atoms
 Mn atoms
(present in
NTC
ceramic)

Figure 4.6: SEM pictures and EDS analysis before and after maximum pressure was applied on sample A.

4.3 Electrode design influence

In figure 4.7, the ansys simulations for all the designs are shown. As expected, the spiral design shows the weakest field distribution whereas the spike design shows the highest (due to the sharp tips). The rest of designs show similar values so a proper distinction can not be done. As this simulation was meant for a qualitative comparison rather than a quantitative comparison, what is being looked for is if there is a specific design that could potentially enhance the electrical performance.

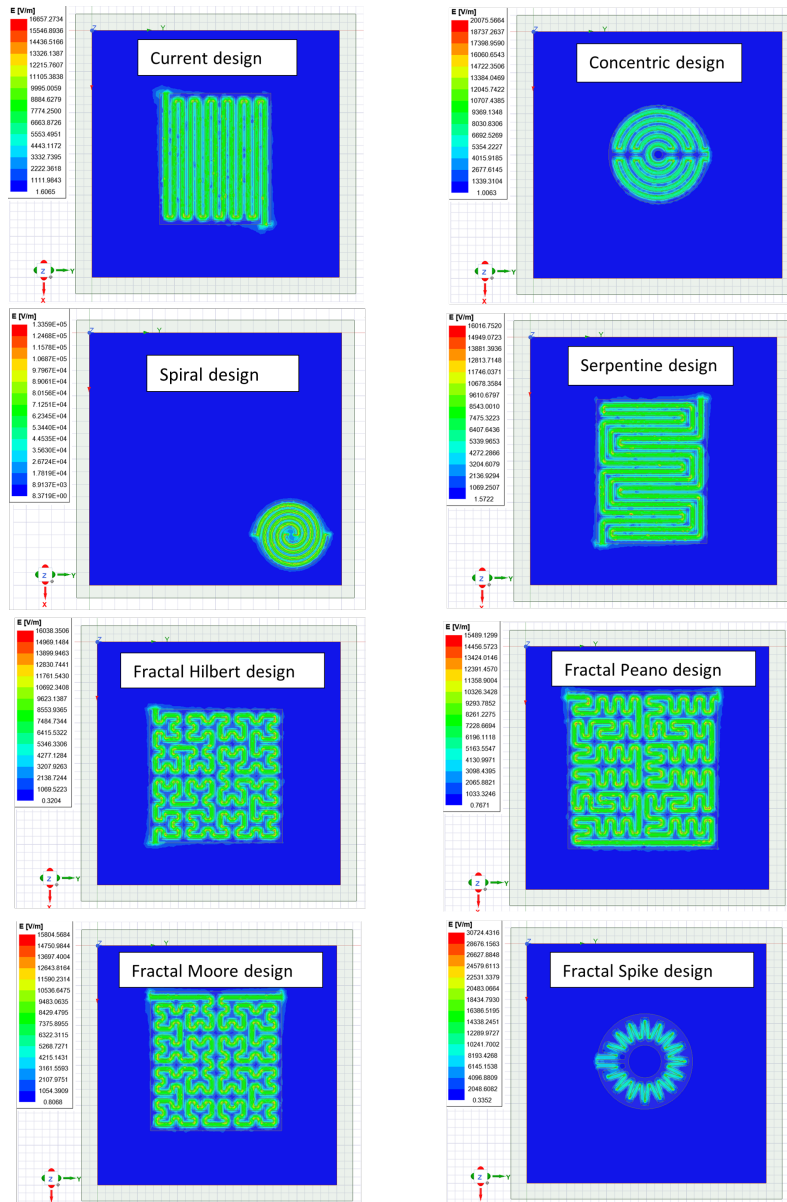


Figure 4.7: Electric field simulation with different electrodes designs.

In figure 4.8, behavior of every design at different voltages is shown (average from the 3 samples prepared per design). Similarly to the simulation, the spiral design

has the highest resistivity (or lowest electrical performance). Most of the other designs have better conductivity than the standard IDE (except the serpentine) which could not be properly concluded in the simulation. However, the spike design does not show the best conductivity expected from the strongest electric field distribution in the simulations.

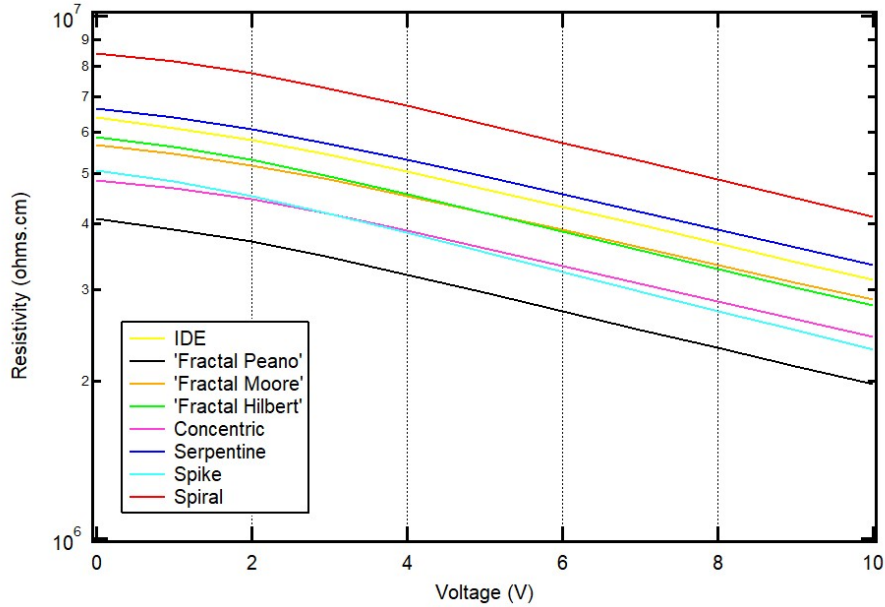


Figure 4.8: Resistivity vs Voltage for all electrode designs.

4.4 Humidity stability

In figure 4.9, it can be seen that the resistance follows the humidity behavior even though the temperature inside the chamber is kept the same. Referring to the change of resistance between 50 *RH*% and 90 *RH*%, it is of 3 % approximately (this is an average from the 3 samples tested). Furthermore, after the humidity cycle was completed, there is a shift of resistance of 7 % from its starting value (this is an average as well from the 3 samples tested).

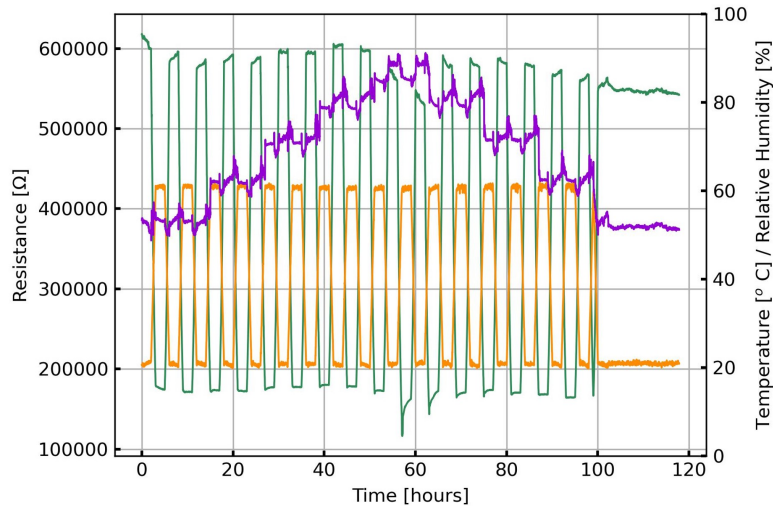


Figure 4.9: Resistance measurement during climatic chamber cycle of epoxy-ceramic NTC thermistor with silver electrodes. Temperature is in orange, resistance measured is in green and humidity is in purple.

In figure 4.10, it can be seen that the resistance still follows the humidity behavior even though the temperature inside the chamber is kept the same. Referring to the change of resistance between 50 *RH*% and 90 *RH*%, it is of 1.5 % approximately (this is an average from the 3 samples tested). Furthermore, after the humidity cycle was completed, there is a shift of resistance of 6.5 % from its starting value (this is an average as well from the 3 samples tested).

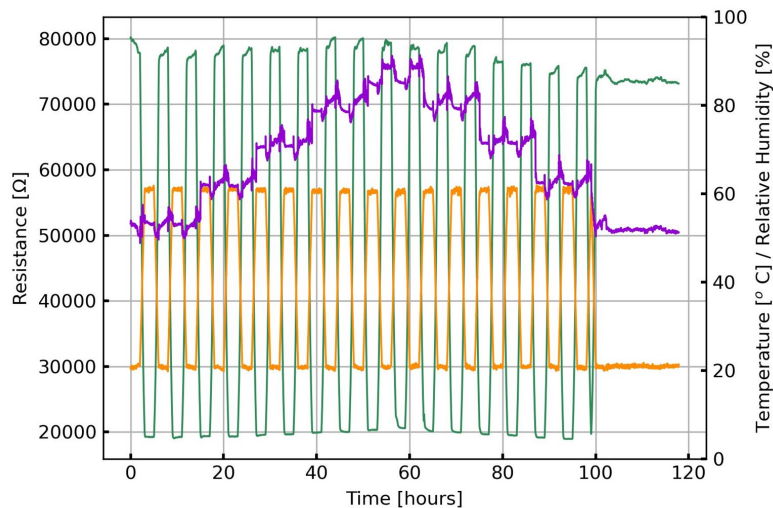


Figure 4.10: Resistance measurement during climatic chamber cycle of epoxy-ceramic NTC thermistor with nickel gold electrodes. Temperature is in orange, resistance measured is in green and humidity is in purple.

5 DISCUSSION

5.1 Percolation limit

From the percolation graph, figure 4.1, it can be estimated that the percolation limit should be between 35 and 40 % of ceramic volume. Even though there is not a clear or sudden switch from a conductor behavior, large ceramic concentration, into an insulator behavior, large epoxy concentration, the trend is towards high resistivity for percentages below 40. This differs from Holst Centre's original formulation with the cyclotene as binder. Any future change in the binder material implies going through the same systematic approach as in the percolation limit section to understand how the ceramic powder will disperse in the binder matrix. As to the current epoxy solution, 40 % of ceramic volume is the ideal formulation. However, this formulation is suitable for stencil-printing applications. If screen-printing is wanted, a new epoxy solution should be looked into as the ink is still too thick for automated screen-printing.

It is important to note as well that with this formulation, the Beta coefficient is of approximately 3400K, which is the same as Holst Centre's original NTC thermistor [15]. This means that the main electrical properties of the ceramic powder were still kept even though the binder was changed.

From the Lichtenecker model, getting a degree of connectivity in between the upper and lower limit, correlates to the randomness of the ceramic powder dispersion in the epoxy matrix after mixture in the planetary mixer. This can lead to issues when trying to launch a commercial sensor, since the random mixture will differ from batch to batch and will affect the R25 from batch to batch as well. This does not mean that the thermistor will not work properly, but it implies that individual calibration curves will be needed. Stabilizing the mixture process is a crucial step before thinking of a commercial product.

Finally, the SEM pictures showed how critical the formation of conduction paths between ceramic particles are because of the direct effect they have on the resistivity and, therefore, the electrical performance of the device.

5.2 Pressure influence

Reason for the breakage of the conduction paths, seen in the SEM pictures, from pressure can be attributed to the NTC layer being too brittle. This is important to point out as it means the sensor is susceptible to loss of performance if it is not mounted with caution on the surface of a system it is supposed to be measuring its temperature (this applies to any housing or encapsulation mounted directly on the NTC region as well).

Furthermore, from the theoretical part, it was possible to improve the electrical performance of the device with external pressure applied, but from the tests it is clear that the opposite scenario is more likely to happen. In order to push particles closer together, a different setup should be taken into account.

5.3 Electrode influence

Electrode design does have an effect on the electrical performance of the device, mainly from 2 factors: increasing the active region in the smallest possible area and improving the electrical flux at sites shaped for a higher electric field distribution (edging effect). This was specifically seen with the spiral design as it had an uniform electric field along the its whole active region that translated into having the worst in conductivity.

With the spike design, even though there is improvement in the conductivity, it was not as dramatic as shown in the simulations. This can be explained from the fact that the strong electric field simulated at the sharp tips are small when compared to the distance of 300 μm between electrodes, thus, it can not be fully used to improve the charge carrier mobility from the tips to the opposite electrode.

On the other hand, the fractal Peano design had the best conductivity. This could be explained due to having a larger electrode area than the other designs and, as a consequence, having several spots of high electric field in its fingers that can be fully used by the NTC layer.

Additionally, if the electrode design can help enhance the electrical properties of the thermistor, it means a higher amount of epoxy can be included in the formulation so that the mechanical properties improve (more flexibility) without compromising the electrical part.

5.4 Humidity stability

Even though the humidity effect on the NTC thermistor could not be completely overcome with the epoxy binder, the degree of influence was lowered down in both initial irreversible shift in resistance (from 8 % to 7 % approximately) and change in resistance at 90 *RH*% (from 5 % to 3 % approximately). The epoxy helped encapsulating the device but it is too thin and not sufficient. An external encapsulation layer or humidity barrier is needed.

As for the nickel gold electrodes, the performance is much better than the silver electrodes, though still it is affected by humidity. However, this can be attributed to the NTC layer rather than the electrodes because they did not suffer from oxidation as in the case of the silver electrodes (seen by the change of color in the silver tracks). Gold is an optimal material for this application but in terms of cost could become an obstacle when industrialization of the sensor is needed.

Only when the resistance change, due to humidity, is below 1 %, the device can be properly industrialized as this tolerance competes with current industry sensors in terms of lifetime and aging behavior.

6 CONCLUSIONS

An epoxy-ceramic based NTC thermistor is a suitable option for lowering down the curing temperature and get access to a wider range of flexible substrates (PEN, PET) without comprising the electrical performance of the original formulation (Beta coefficient of 3400K).

The influence of the amount of the ceramic power in the binary composite was understood and a systematic approach to find an optimal formulation when the composite changes was found (percolation limit).

External pressure was found to be harmful for this specific epoxy solution due to the NTC's brittle nature.

The electrode design can be used to enhance electrical properties of the thermistor when the binder properties are strong in the composite.

Role of the electrode material in high humidity conditions was understood and quantified. Encapsulation properties from the epoxy binder were found to be insufficient to act as a humidity barrier so further protection is needed.

Bibliography

- [1] Antonio Feteira. “Negative Temperature Coefficient Resistance (NTCR) Ceramic Thermistors: An Industrial Perspective”. In: *Journal of the American Ceramic Society* 92.5 (2009), pp. 967–983. DOI: <https://doi.org/10.1111/j.1551-2916.2009.02990.x>. eprint: <https://ceramics.onlinelibrary.wiley.com/doi/pdf/10.1111/j.1551-2916.2009.02990.x>. URL: <https://ceramics.onlinelibrary.wiley.com/doi/abs/10.1111/j.1551-2916.2009.02990.x>.
- [2] Farnell Ltd. *A guide to temperature sensor design*. 2018. URL: <https://nl.farnell.com/a-guide-to-temperature-sensor-design> (visited on 03/15/2022).
- [3] Wikipedia. *Thermocouple*. URL: <https://en.wikipedia.org/wiki/Thermocouple> (visited on 03/15/2022).
- [4] DSPE. *Semiconductor temperature sensors*. URL: <https://www.dspe.nl/knowledge/thermomechanics/chapter-5-measurement/5-2-contact-sensors/5-2-6-semiconductor-temperature-sensors/> (visited on 03/15/2022).
- [5] Circuit Globe. *Difference Between RTD Thermistor*. URL: <https://circuitglobe.com/difference-between-rtd-and-thermistor.html> (visited on 03/15/2022).
- [6] Ametherm. *NTC Thermistor Temperature Sensors Provide Li-Ion Battery Safety*. URL: <https://www.ametherm.com/blog/thermistors/thermistors-ntc-thermistor-temperature-sensors-provide-li-ion-battery-safety/> (visited on 03/16/2022).
- [7] Battery University. *BU-409: Charging Lithium-ion*. URL: <https://batteryuniversity.com/article/bu-409-charging-lithium-ion> (visited on 03/16/2022).
- [8] Samuel Ruben. *Electrical pyrometer resistance*. Nov. 1935.
- [9] Schottky Walter. *Thermonegative Resistor*. Dec. 1939.

- [10] Antonio Feteira and Klaus Reichmann. “NTC Ceramics: Past, Present and Future”. In: *12th INTERNATIONAL CERAMICS CONGRESS PART F*. Vol. 67. Advances in Science and Technology. Trans Tech Publications Ltd, Jan. 2011, pp. 124–133. DOI: [10.4028/www.scientific.net/AST.67.124](https://doi.org/10.4028/www.scientific.net/AST.67.124).
- [11] Deutz Daniella. *Structure property relationships for NTC ceramics (I) and polymer composites (II)*. 2013.
- [12] John S. Steinhart and Stanley R. Hart. “Calibration curves for thermistors”. In: *Deep Sea Research and Oceanographic Abstracts* 15.4 (1968), pp. 497–503. ISSN: 0011-7471. DOI: [https://doi.org/10.1016/0011-7471\(68\)90057-0](https://doi.org/10.1016/0011-7471(68)90057-0). URL: <https://www.sciencedirect.com/science/article/pii/0011747168900570>.
- [13] Tran Quang Trung and Nae-Eung Lee. “Flexible and Stretchable Physical Sensor Integrated Platforms for Wearable Human-Activity Monitoring and Personal Healthcare”. In: *Advanced Materials* 28.22 (2016), pp. 4338–4372. DOI: <https://doi.org/10.1002/adma.201504244>. eprint: <https://onlinelibrary.wiley.com/doi/pdf/10.1002/adma.201504244>. URL: <https://onlinelibrary.wiley.com/doi/abs/10.1002/adma.201504244>.
- [14] Qiao Li, Li-Na Zhang, Xiao-Ming Tao, et al. “Review of Flexible Temperature Sensing Networks for Wearable Physiological Monitoring”. In: *Advanced Healthcare Materials* 6.12 (2017), p. 1601371. DOI: <https://doi.org/10.1002/adhm.201601371>. eprint: <https://onlinelibrary.wiley.com/doi/pdf/10.1002/adhm.201601371>. URL: <https://onlinelibrary.wiley.com/doi/abs/10.1002/adhm.201601371>.
- [15] Dimitra Katerinopoulou, Peter Zalar, Jorgen Sweelssen, et al. “Large-Area All-Printed Temperature Sensing Surfaces Using Novel Composite Thermistor Materials”. In: *Advanced Electronic Materials* 5.2 (2019), p. 1800605. DOI: <https://doi.org/10.1002/aelm.201800605>. eprint: <https://onlinelibrary.wiley.com/doi/pdf/10.1002/aelm.201800605>. URL: <https://onlinelibrary.wiley.com/doi/abs/10.1002/aelm.201800605>.
- [16] *NTC Thermistors*. R44E. Rev. 1. Murata. Mar. 2020.
- [17] Kyung-Soon Park and J. Lee. “The effect of ZnO content and sintering temperature on the electrical properties of Cu-containing $\text{Mn}_{1.95}\text{Ni}_{0.45}\text{Co}_{0.15}\text{Cu}_{0.45}\text{Zn}_x$ ($0 \leq x \leq 0.3$) NTC thermistors”. In: *Journal of Alloys and Compounds* 475 (May 2009), pp. 513–517. DOI: [10.1016/j.jallcom.2008.07.076](https://doi.org/10.1016/j.jallcom.2008.07.076).

- [18] K. Park and J.K. Lee. “MnNiCoCuZnO NTC thermistors with high thermal stability for low resistance applications”. In: *Scripta Materialia* 57.4 (2007), pp. 329–332. ISSN: 1359-6462. DOI: <https://doi.org/10.1016/j.scriptamat.2007.04.026>. URL: <https://www.sciencedirect.com/science/article/pii/S1359646207003119>.
- [19] J. L. Martín De Vidales, P. Garcia-Chain, Rosa M. Rojas, et al. “Preparation and characterization of spinel-type MnNiCoO negative temperature coefficient ceramic thermistors”. In: *Journal of Materials Science* 33 (1998), pp. 1491–1496.
- [20] *Report on Improved Temperature Sensor*. D3.1.4. Rev. 1. Holst Centre. Jan. 2020.
- [21] Yi-Fei Wang, Tomohito Sekine, Yasunori Takeda, et al. “Fully Printed PEDOT:PSS-based Temperature Sensor with High Humidity Stability for Wireless Healthcare Monitoring”. In: *Scientific Reports* 10 (Feb. 2020). DOI: [10.1038/s41598-020-59432-2](https://doi.org/10.1038/s41598-020-59432-2).
- [22] Ltd DONGGUAN XINGLEKUN SHAN) Electrical Insulation Material Co. *Teonex PEN Film*. URL: <http://www.mylar-nmn.com/product/276504170> (visited on 05/10/2022).
- [23] PAC. *Resistivity Test Methods*. URL: <https://www.gotopac.com/art-esd-resistivity> (visited on 05/17/2022).
- [24] O. Aleksic, B. Radojicic, and R. Ramovic. “Electrode Effect on NTC Planar Thermistor Volume Resistivity”. In: *2006 25th International Conference on Microelectronics*. 2006, pp. 580–583. DOI: [10.1109/ICMEL.2006.1651033](https://doi.org/10.1109/ICMEL.2006.1651033).
- [25] James E. Tyrrell, Martyn G. Boutelle, and Alasdair J. Campbell. “Measurement of Electrophysiological Signals In Vitro Using High-Performance Organic Electrochemical Transistors”. In: *Advanced Functional Materials* 31.1 (2021), p. 2007086. DOI: <https://doi.org/10.1002/adfm.202007086>. eprint: <https://onlinelibrary.wiley.com/doi/pdf/10.1002/adfm.202007086>. URL: <https://onlinelibrary.wiley.com/doi/abs/10.1002/adfm.202007086>.
- [26] D B Deutz, S van der Zwaag, and P Groen. “Effect of particle contact on the electrical performance of NTC-epoxy composite thermistors”. In: *Materials Research Express* 7.2 (Feb. 2020), p. 025702. DOI: [10.1088/2053-1591/ab706d](https://doi.org/10.1088/2053-1591/ab706d). URL: <https://doi.org/10.1088/2053-1591/ab706d>.

- [27] David S. McLachlan, Michael Blaszkiewicz, and Robert E. Newnham. “Electrical Resistivity of Composites”. In: *Journal of the American Ceramic Society* 73.8 (1990), pp. 2187–2203. DOI: <https://doi.org/10.1111/j.1151-2916.1990.tb07576.x>. eprint: <https://ceramics.onlinelibrary.wiley.com/doi/pdf/10.1111/j.1151-2916.1990.tb07576.x>. URL: <https://ceramics.onlinelibrary.wiley.com/doi/abs/10.1111/j.1151-2916.1990.tb07576.x>.
- [28] A.V. Goncharenko, V.Z. Lozovski, and E.F. Venger. “Lichtenecker’s equation: applicability and limitations”. In: *Optics Communications* 174.1 (2000), pp. 19–32. ISSN: 0030-4018. DOI: [https://doi.org/10.1016/S0030-4018\(99\)00695-1](https://doi.org/10.1016/S0030-4018(99)00695-1). URL: <https://www.sciencedirect.com/science/article/pii/S0030401899006951>.
- [29] Zhi-Yuan Ling and Lin He. “Thick-Film Negative-Temperature-Coefficient Thermistors with a Linear Resistance-Temperature Relation”. In: *Chinese Physics Letters* 30.10 (Oct. 2013), p. 107201. DOI: [10.1088/0256-307x/30/10/107201](https://doi.org/10.1088/0256-307x/30/10/107201). URL: <https://doi.org/10.1088/0256-307x/30/10/107201>.
- [30] Kiranmai Uppuluri and Dorota Szwagierczak. “Fabrication and characterization of screen printed NiMn 2 O 4 spinel based thermistors”. In: *Sensor Review* ahead-of-print (Jan. 2022). DOI: [10.1108/SR-07-2021-0218](https://doi.org/10.1108/SR-07-2021-0218).
- [31] Taichi Kikkawa, Daisuke Kumaki, Shizuo Tokito, et al. “Nickel oxide-based flexible thin-film NTC thermistors by using reverse offset printing”. In: *Flexible and Printed Electronics* 7.1 (Jan. 2022), p. 015003. DOI: [10.1088/2058-8585/ac489f](https://doi.org/10.1088/2058-8585/ac489f). URL: <https://doi.org/10.1088/2058-8585/ac489f>.
- [32] Jan Kulawik, Dorota Szwagierczak, B. Gröger, et al. “Fabrication and characterization of bulk and thick film perovskite NTC thermistors”. In: *Microelectronics International* 24 (Apr. 2007), pp. 14–18. DOI: [10.1108/1356536071074554](https://doi.org/10.1108/1356536071074554).
- [33] Ruping Liu, Liang He, Meijuan Cao, et al. “Flexible Temperature Sensors”. In: *Frontiers in Chemistry* 9 (2021). ISSN: 2296-2646. DOI: [10.3389/fchem.2021.539678](https://doi.org/10.3389/fchem.2021.539678). URL: <https://www.frontiersin.org/articles/10.3389/fchem.2021.539678>.
- [34] Almudena Rivadeneyra, José Fernández-Salmerón, Jesús Banqueri, et al. “A novel electrode structure compared with interdigitated electrodes as capacitive sensor”. In: *Sensors and Actuators B: Chemical* 204 (2014), pp. 552–560. ISSN: 0925-4005. DOI: <https://doi.org/10.1016/j.snb.2014.08.010>. URL: <https://www.sciencedirect.com/science/article/pii/S0925400514009782>.

- [35] L. E. B. Ribeiro and Fabiano Fruett. “Analysis of the Planar Electrode Morphology for Capacitive Chemical Sensors”. In: 2015.
- [36] *Critical Parameters of the Electrorheological Effect*. vol.2. p. 283302. SUKIENNIK, M. and POCHARSKI, Janusz. 2011.
- [37] Sumana Kumar, Swanand Telpande, Veera Manikandan, et al. “Novel electrode geometry for high performance CF/Fe₂O₃ based planar solid state micro-electrochemical capacitors”. In: *Nanoscale* 12 (37 2020), pp. 19438–19449. DOI: 10.1039/D0NR04410E. URL: <http://dx.doi.org/10.1039/D0NR04410E>.
- [38] Aashir Waheed Syed and Mohammad Ali Mohammad. “Laser Scribed Graphene-Based Flexible Microsupercapacitors With Fractal Design”. In: *IEEE Access* 9 (2021), pp. 154957–154964. DOI: 10.1109/ACCESS.2021.3128320.
- [39] Paul Goodman. “Current and future uses of gold in electronics”. In: *Gold Bulletin* 35 (Mar. 2002), pp. 21–26. DOI: 10.1007/BF03214833.